

**Streamwise turbulence modulation in non-uniform open-channel clay suspension flows**

de Vet, M.G.W. ; Fernandez, R.; Baas, Jaco H.; McCaffrey, William D.; Dorrell, Robert M.

Journal of Geophysical Research: Earth Surface

DOI:
[10.1029/2022JF006781](https://doi.org/10.1029/2022JF006781)

E-pub ahead of print: 26/07/2023

Peer reviewed version

[Cyswllt i'r cyhoeddiad / Link to publication](#)

Dyfyniad o'r fersiwn a gyhoeddwyd / Citation for published version (APA):
de Vet, M. G. W., Fernandez, R., Baas, J. H., McCaffrey, W. D., & Dorrell, R. M. (2023). Streamwise turbulence modulation in non-uniform open-channel clay suspension flows. *Journal of Geophysical Research: Earth Surface*, [e2022JF006781].
<https://doi.org/10.1029/2022JF006781>

Hawliau Cyffredinol / General rights

Copyright and moral rights for the publications made accessible in the public portal are retained by the authors and/or other copyright owners and it is a condition of accessing publications that users recognise and abide by the legal requirements associated with these rights.

- Users may download and print one copy of any publication from the public portal for the purpose of private study or research.
- You may not further distribute the material or use it for any profit-making activity or commercial gain
- You may freely distribute the URL identifying the publication in the public portal ?

Take down policy

If you believe that this document breaches copyright please contact us providing details, and we will remove access to the work immediately and investigate your claim.

1 **Streamwise turbulence modulation in non-uniform open-channel clay suspension**
2 **flows**

3 **M.G.W. de Vet¹, R. Fernández^{1,2}, J.H. Baas³, W.D. McCaffrey⁴ and R. M. Dorrell¹**

4 ¹ Energy and Environment Institute, University of Hull. Hull HU6 7RX, U.K.

5 ² Department of Civil and Environmental Engineering, Penn State University. University Park,
6 PA 16802, USA.

7 ³ School of Ocean Sciences, Bangor University, Menai Bridge, Anglesey LL59 5AB, U.K.

8 ⁴ School of Earth and Environment, University of Leeds, Leeds LS2 9 JT, U.K.

9
10 Corresponding author: Marijke de Vet (m.de-vet@hull.ac.uk)

11 **Key Points:**

- 12 • Comparable to uniform flow, the combination of flow velocity and clay concentration
13 influences the clay flow type in non-uniform flows
- 14 • Accelerating clay-laden flows adapt faster to velocity changes than decelerating flows;
15 breaking clay bonds is easier than establishing them
- 16 • Adaptation timescales grow with clay concentration for decelerating clay-laden flows
17 passing through a larger variety of clay flow types

18
19

20 Abstract

21 Cohesive sediment particles are ubiquitous in environmental flows. The cohesive properties of
22 clay promote the formation of clay flocs and gels and relatively small suspended clay
23 concentrations can enhance or suppress turbulence in a flow. Furthermore, flows are naturally
24 non-uniform, varying in space and time, yet the dynamics of non-uniform open-channel clay
25 suspension flows is poorly understood. For the first time, the adaptation time and length scales of
26 non-uniform clay suspension flows were quantified using novel experiments with spatially
27 varying, but temporally uniform flow. Different levels of turbulence enhancement and
28 attenuation were identified as the flow decelerates or accelerates. Results highlight that
29 decelerating clay suspension flows crucially have a longer adaptation time than accelerating clay
30 suspension flows. This is explained by the longer timescale required for formation of bonds
31 between cohesive particles in turbulence attenuated flows after deceleration than the rapid
32 breakdown of bonds in turbulent flows after acceleration of clay suspension flows. This
33 hysteresis is more pronounced for higher concentration decelerating flows that pass through a
34 larger variety of clay flow types of turbulence enhancement and attenuation. These different
35 adaptation time scales and associated clay flow type transitions are likely to affect clay flow
36 dynamics in a variety of fluvial and submarine settings.

37 Plain Language Summary

38 Flows in natural environments, such as rivers, estuaries, seas, and oceans, can transport sediment
39 in suspension. The suspended sediment can increase or decrease turbulence in a flow, depending
40 on the sediment concentration. Clay has the ability to form bonds between the individual
41 particles and therefore even small concentrations are sufficient to alter turbulence levels in a
42 flow. The amount of alteration of turbulence is known for uniform, constant flow conditions, but
43 in natural environments, flows are often non-uniform. For example, flow variations can occur
44 due to changes in river width or bed slope. The influence of these variations on clay suspension
45 flows is unknown. New physical experiments were conducted where clay suspension flows were
46 decelerated and accelerated. As the flow decelerates, turbulence in the flow is reduced and bonds
47 between the suspended clay particles are established. Turbulence increases as the flow
48 accelerates and clay bonds are broken. Decelerating flow requires more time to adjust to changes
49 in velocity than accelerating flow, as establishing the bonds between clay particles requires more
50 time than breaking them. This means that, especially for the decelerating flows, the influence of
51 a change in velocity is noticeable further downstream.

52 1 Introduction

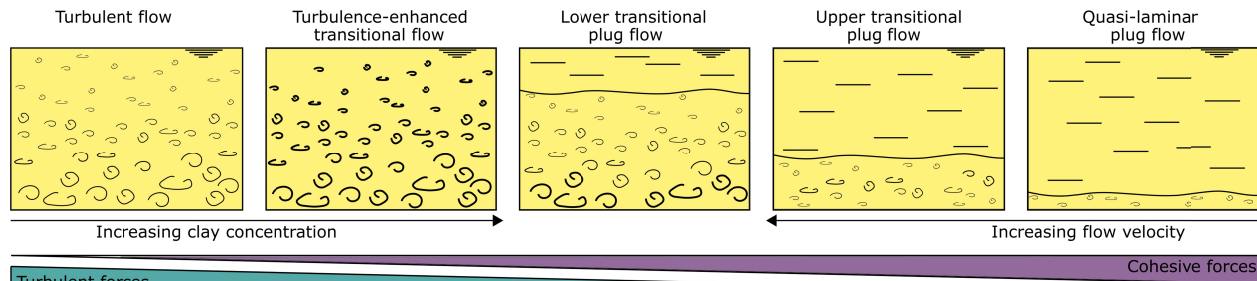
53 Cohesive sediment-laden flows are important in a wide range of natural environments, such as
54 rivers, estuaries, shallow seas and deep oceans (Whitehouse et al., 2000; Winterwerp and van
55 Kesteren, 2004), and in industrial settings (Ackers et al., 2001). For example, cohesive sediment
56 supply to rivers can be increased by high-magnitude, low-frequency events, such as storms,
57 floods and post-wildfire erosion (Swanson, 1981; Sankey et al., 2017), which occur more often
58 because of climate change (Geertsema et al., 2006; Reneau et al., 2007; Barbero et al., 2015).
59 Furthermore, cohesive sediment is common in submarine gravity currents, such as turbidity
60 currents, hybrid events, mass flows and associated deposits (Talling et al., 2012). The increases
61 in sediment transport can have major impacts on water quality and aquatic ecosystems, including
62 fish habitats, and channel morphology (Smith et al., 2011). High suspended cohesive sediment

63 concentrations modify flow dynamics by either enhancing (Best et al., 1997; Baas and Best,
64 2002) or dampening turbulence (Bagnold, 1954; Wang and Larsen, 1994), influencing sediment
65 transport rates and erosion and deposition patterns (Partheniades, 1965; Metha et al., 1989).

66
67 Cohesive clay particles may collide and form larger particles, or flocs, when the distance
68 between the particles is sufficiently small (Van Olphen, 1977; Winterwerp and van Kesteren,
69 2004). Networks of flocs in the flow, i.e., clay gels, enhance viscosity and yield stress, and thus
70 are a key control on flow turbulence (Baas and Best, 2002). Research into steady, uniform clay
71 flows indicate a close interaction between turbulent and cohesive forces, controlling the dynamic
72 structure of clay flows (Baas and Best, 2002; Baas et al., 2009). As the clay concentration
73 increases, it becomes increasingly difficult to break the cohesive bonds between particles,
74 resulting in the formation of a pervasive network of permanently interlinked clay particles;
75 turbulent energy is dissipated by the high effective viscosity, and the flow becomes laminar.
76 Conversely, the electrostatic bonds between the clay particles can be broken in regions of high
77 shear. Thus, an increase in turbulence generation in the flows by, for example, an increasing flow
78 velocity has the potential to break bonds between the clay particles and reduce the flow viscosity
79 (Partheniades, 2009). This shifting balance between turbulent and cohesive forces regulates the
80 dynamic structure of cohesive flows (Baas et al., 2009).

81
82 Baas et al. (2009) defined a clay flow classification scheme based on flume experiments. The
83 only technique available for velocity measurements in high concentrated flows is Ultrasonic
84 Velocity Profilers, which are designed to work along a single beam. This allows velocity
85 measurements to be collected in one flow direction and consequently, Baas et al. (2009) based
86 the clay flow classification scheme on streamwise velocity measurements instead of a 3D
87 turbulence field. The clay flow classification scheme consists of five different clay flow types in
88 order of increasing clay concentration: turbulent flow, turbulence-enhanced transitional flow,
89 lower transitional plug flow, upper transitional plug flow, and quasi-laminar plug flow (Fig. 1).
90 Turbulent flow exhibits a logarithmic velocity profile with an associated decrease in turbulence
91 intensity away from the bed (Nezu and Nakagawa, 1993). The velocity of turbulence-enhanced
92 transitional flows progressively diminishes, in particular close to the base of the flow,
93 accompanied by a progressive increase in turbulence intensity over the full flow depth, whilst the
94 logarithmic velocity profile is maintained. A progressive increase in clay concentration in lower
95 transitional plug flows results in the formation of a plug, which thickens from the water surface
96 downwards. This flow type exhibits a decreased near-bed velocity and increased near-bed
97 turbulence in combination with decreased turbulence intensity in the outer flow. The plug flow
98 further thickens downwards in upper transitional plug flows with increasing clay concentration,
99 whilst the maximum turbulence intensity moves away from the bed and decreases. The upward
100 shift in turbulence production is explained through thickening of the viscous sublayer (Best and
101 Leeder, 1993; Li and Gust, 2000) and the development of an internal shear layer (Baas and Best,
102 2002), which separates the near-bed region from the plug flow region. Further increasing the clay
103 concentration results in fully suppressed turbulence in quasi-laminar plug flows, apart from
104 minor residual turbulence near the base of the flow in a thin shear layer.

105



106
107 Figure 1. Schematic model of the balance between cohesive and turbulent forces that determines
108 the behaviour of turbulent, transitional, and laminar clay-laden flows, divided into five different
109 clay flow types after the classification scheme of Baas et al. (2009). Modified after Baas et al.
110 (2009).

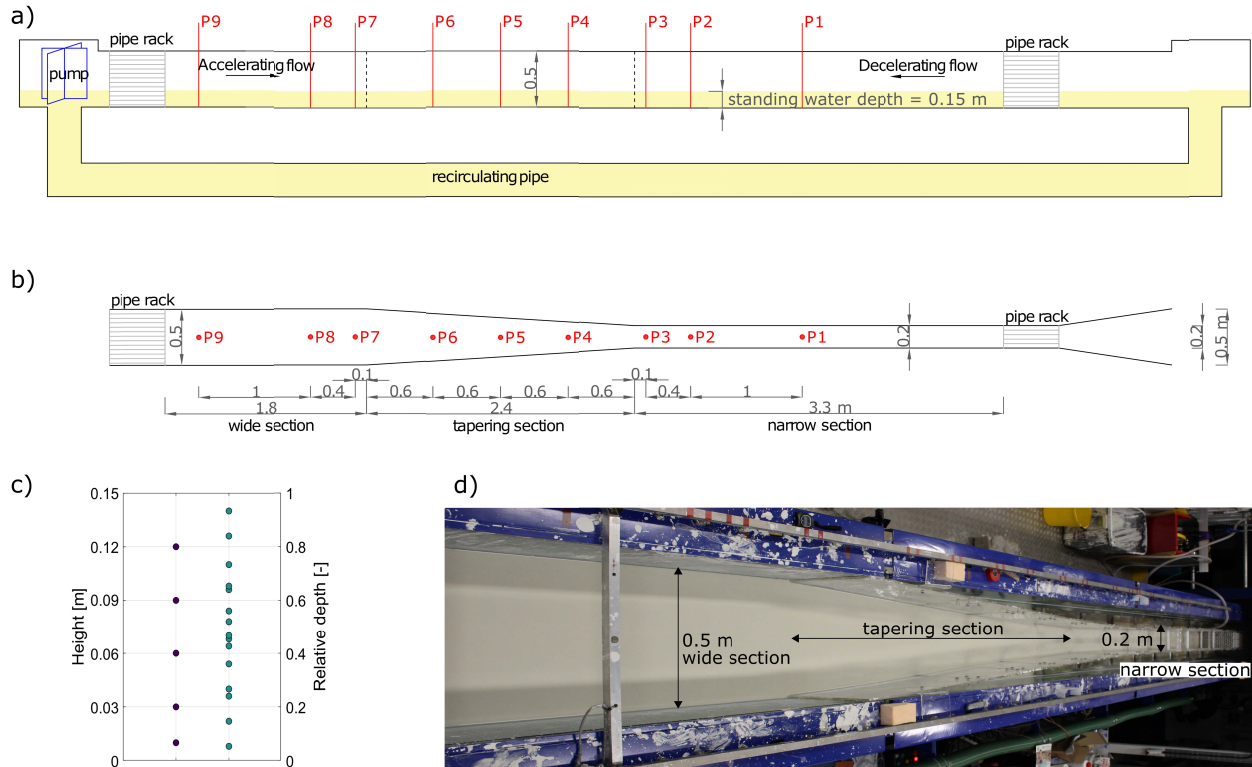
111
112 Flows are naturally non-uniform; here, flow non-uniformity is taken to refer to streamwise
113 changes in depth-averaged velocity. The effect of clay on streamwise decelerating and
114 accelerating flow is essential for understanding sediment-laden flow dynamics. The formation of
115 bonds between cohesive sediment particles is a time-dependent (thixotropic) process and,
116 therefore, cohesive-sediment laden flows need time to adjust to spatial variations in flow
117 velocity. However, the changing balance between turbulent and cohesive forces in clay-laden
118 flows under non-uniform conditions is poorly understood. Understanding this balance is pivotal,
119 as erosion, transport, and deposition of sediment depend on the magnitude and distribution of
120 flow turbulence (Dorrell et al., 2018). Spatio-temporal increases and decreases in turbulence
121 directly affect the transport capacity and deposition and erosion patterns (Dorrell and Hogg,
122 2012; Moody et al., 2013).

123
124 An increased understanding of the influence of cohesive sediment on non-uniform flow
125 conditions is needed. This paper details experimental results on the flow structure of clay-laden
126 flows, for the first time isolating the effect of non-uniformity by spatial deceleration and
127 acceleration in open-channel flows. The aim is to understand the adaptation of clay-laden flows
128 to non-uniform flow conditions. We address the following research questions: (1) What are the
129 mean flow and streamwise turbulence characteristics of horizontally decelerating and
130 accelerating clay-laden flows (Section 3)? (2) How do non-uniform flows with different
131 suspended clay concentration compare to each other and to uniform clay-laden flows, i.e. which
132 clay flow types can be identified in clay-laden decelerating and accelerating flows (Section 4.1)?
133 (3) How much time do decelerating and accelerating flows need to adapt to the changing flow
134 conditions (Section 4.2)? (4) Are there differences in adaptation between decelerating and
135 accelerating clay-laden flows (Section 4.3)?

136 2 Methodology

137 Mixtures of pure kaolinite (Imerys Polwhite-E, median particle size $D_{50} = 9 \mu\text{m}$, sediment
138 density $\rho_s = 2600 \text{ kg m}^{-3}$) and fresh water were circulated through a horizontal hydraulic flume
139 by means of a variable-discharge slurry pump (Fig. 2a). The flume was 10 m long and 0.5 m
140 wide, with a standing water depth, h_0 , of 0.15 m. At the upstream end, the flume contained a
141 turbulence-damping grid to straighten the flow. The flow moved over a flat, smooth floor
142 downstream of the turbulence-damping grid. An inset channel was placed in the flume. It had a
143 0.2 m wide narrow section and a 2.4 m long tapering section. This division in the flume results in
144 a flume expansion or narrowing with a ratio of 1 to 16; this smooth transition avoided flow

145 separation or recirculation cells. The inset forced the flow through a narrow to wide transition
 146 (decelerating flows) or through a wide to narrow transition (accelerating flows) depending on the
 147 flow direction (Fig. 2b). Thus, in contrast to earlier work in non-tapering flumes (Baas and Best,
 148 2002; Baas et al., 2009), this channel design enabled controlled spatial changes in the flow
 149 velocity and turbulence to be measured.
 150



151
 152 Figure 2. a) Side view of the experimental setup, b) top view of the inset channel, with points P
 153 indicating measurement locations, c) velocity (U) and sediment concentration (C) measurement
 154 positions above the channel bed; relative depth = height / depth, d) photo of the flume setup. All
 155 dimensions in meters.
 156

157 2.1 Experimental conditions

158 Table 1 shows the range of clay concentrations and flow velocities used; control experiments
 159 were conducted with clear water. Clay was soaked in water for a minimum of one day before
 160 adding the clay suspension to the flume, to guarantee that no dry clumps remained. To ensure a
 161 uniform mixture of clay and water in the flume, initially, the flume was run at high rotational
 162 speed of the slurry pump for 30 minutes combined with additional mixing in the wide section
 163 using a hand-held mixture. Afterwards, the flume ran for 16 to 20 hours to allow the clay-laden
 164 flows to reach equilibrium conditions and allow for any deposition of clay before measurements
 165 were taken. This allowed assessment of streamwise turbulence dynamics of non-uniform clay-
 166 laden flows without influence of erosional or depositional processes. Control measurements of
 167 the velocity were collected 3 hours after experimental runs to confirm the establishment of
 168 equilibrium conditions.

169

170 Table 1. *Experimental conditions at selected positions in the flume. Q = discharge, based on*
 171 *velocity measurements at P2 with assumed minimal change in velocity over the flume width; C =*
 172 *spatial-averaged volumetric concentration, based on an average of suspended sediment samples*
 173 *over the depth and along the length of the flume; h_0 = standing water depth at P8; T = water*
 174 *temperature; \bar{U} = depth-averaged velocity; Fr = Froude number; Re = Reynolds number. The*
 175 *labelling of experimental runs is defined using D for decelerating and A for accelerating flows*
 176 *and the value of clay concentration.*

Experimental run	Q	C	h_0	T	Measuring point	\bar{U}	Fr	Re
	[m ³ /s]	[vol %]	[m]	[°C]		[m/s]	[-]	[- · 10 ⁴]
<i>Decelerating flow</i>								
D1-C0.0	0.021	0.00	0.150	16.0	P2	0.69	0.57	10.3
					P5	0.52	0.43	7.8
					P8	0.33	0.27	4.9
D2-C0.0	0.015	0.00	0.158	17.6	P2	0.49	0.40	7.8
					P5	0.38	0.30	5.9
					P8	0.28	0.23	4.5
D3-C0.9	0.014	0.92	0.150	18.7	P2	0.48	0.39	6.7
					P5	0.35	0.29	4.9
					P8*	0.28	0.23	4.0
D4-C1.5	0.019	1.47	0.150	18.0	P2	0.64	0.53	8.3
					P5	0.45	0.37	6.0
					P8	0.33	0.27	4.3
D5-C2.7	0.016	2.67	0.150	18.0	P2	0.54	0.45	5.8
					P5	0.42	0.35	4.5
					P8	0.27	0.22	2.9
<i>Accelerating flow</i>								
A1-C0.0	0.015	0.00	0.170	17.6	P2	0.45	0.35	7.6
					P5	0.26	0.20	4.4
					P8	0.16	0.13	2.7
A2-C1.4	0.014	1.39	0.170	18.0	P2	0.41	0.32	6.2
					P5	0.26	0.20	3.9
					P8*	0.20	0.17	3.0
A3-C1.5	0.016	1.54	0.185	18.7	P2	0.43	0.32	6.9
					P5	0.27	0.20	4.3
					P8*	0.20	0.15	2.3
A4-C2.8	0.015	2.77	0.180	18.2	P2	0.41	0.31	5.1
					P5	0.31	0.23	3.8
					P8*	0.20	0.15	2.5
* deposition was observed at this location								

177

178 2.2 Data acquisition

179 At the start of each run, the water temperature was measured with a thermometer and the water
 180 depth was measured with a ruler at P8. A vertical rack of siphon tubes was used to
 181 synchronously collect 60 ml samples over a duration of 2 minutes at five different heights in the
 182 water column and at three locations for the decelerating (P3, P5, P9) and accelerating (P1, P5,
 183 P7) flows (Fig. 2b, c). The three locations covered the longest lengths possible in the flume for
 184 development of either decelerating or accelerating flow. Hence, the measurement locations
 185 included the first measurement point upstream of the tapering section (P3 for decelerating flow,
 186 P7 for accelerating flow), the middle of the tapering section (P5) and the furthest measurement
 187 point downstream of the tapering section (P9 for decelerating flow and P1 for accelerating flow).
 188 The collected samples were weighed and dried to determine their volumetric clay concentration.
 189 The horizontal flow velocity was measured at nine locations along the flume using Ultrasonic
 190 Velocity Profilers facing upstream (Fig. 2b, c) (Takeda, 1991, Best et al., 2001). Ultrasonic
 191 Velocity Profilers measure flow velocity using the Doppler shift, which relies on the use of
 192 pulsed ultrasound echography. A short emission of ultrasound is transmitted from a profiler, and
 193 the same profiler receives the echo reflected from suspended particles in the flow. To determine
 194 the flow velocity, the Doppler shift frequency is determined from several repeated ultrasound
 195 pulses. In these experiments, five 4 MHz probes were stacked on top of each other with a
 196 distance of 14 mm between their centres. The probes collected velocity data for 500 cycles with
 197 a 50 ms delay between probes to avoid measurement interference. The probe array was shifted
 198 vertically to three different heights during the experiment to cover the full flow depth, resulting
 199 in a total of 15 measurement elevations per location (Fig. 2c). Depending on the experimental
 200 conditions, these settings resulted in measurement durations of 174 to 330 s at a temporal
 201 resolution of 2.9 to 1.5 Hz. Velocity measurements taken at 0.03 to 0.05 m from the probe head
 202 were used in the analysis. An overview of the settings of the Ultrasonic Velocity Profilers used
 203 in these experiments is provided in the Supporting Information.

204 2.3 Data processing

205 Artificial noise was removed from the velocity signal by eliminating values three standard
 206 deviations away from a temporal moving mean measured over 31 datapoints. On average, these
 207 spikes accounted for less than 3% of the data. Datapoints were excluded where deposition
 208 occurred. The temporal mean flow velocity, \bar{U} , and its standard deviation, $RMS(u')$, were then
 209 calculated from the time series of instantaneous velocity data at each measurement height (Baas
 210 et al., 2009):

$$\bar{U} = \frac{1}{n} \sum_i^n u_i \quad (1)$$

$$RMS(u') = \sqrt{\frac{1}{n} \sum_i^n (u_i - \bar{U})^2} \quad (2)$$

211 where n is the number of velocity measurements. The coefficient of variation is used as a
 212 dimensionless measure for turbulence intensity (e.g. Baas et al. 2009):

$$RMS(u')_0 = \frac{RMS(u')}{\bar{U}} \cdot 100 \quad (3)$$

213 Depth-averaged velocity was calculated by integrating the time-averaged velocities over the
 214 depth. The integral was numerically evaluated; velocities were set to zero at the bed and
 215 velocities at the water surface were assumed to have the same value as the first measurement
 216 position below that level:

$$\bar{U} = \frac{1}{h_0} \int_0^{h_0} \bar{U} dz \quad (4)$$

217 where z is height above the bed. Depth-averaged turbulence intensity was calculated by
 218 integrating the turbulence intensity values over the depth.

$$\overline{RMS(u')_0} = \frac{1}{h_0} \int_0^{h_0} RMS(u')_0 dz \quad (5)$$

219

220 In the rare occasion that the reflected signal strength of a Ultrasonic Velocity Profiler is not
 221 sufficient to collect accurate velocity measurements, the velocity measurements can result in
 222 unexpected strong velocity fluctuations. A moving mean is not guaranteed to remove these errors
 223 and a second stage of data cleaning is required. These outliers in the processed velocity dataset
 224 were excluded as follows. Data was identified as an outlier when either the flow velocity, \bar{U} , or
 225 its standard deviation $RMS(u')$, was 40% higher or lower than the median value of the six
 226 immediately surrounding measurement points from the nearest upstream and downstream
 227 locations:

$$\frac{|median(\bar{U}_{j-1,i-1}, \bar{U}_{j,i-1}, \bar{U}_{j+1,i-1}, \bar{U}_{j-1,i+1}, \bar{U}_{j,i+1}, \bar{U}_{j+1,i+1}) - \bar{U}_{j,i}|}{\bar{U}_{j,i}} \cdot 100 > 40 \quad (6)$$

228 with i = point, j = height. Here, the median was used to avoid weighting from outliers. At the
 229 outer locations, P1 and P9, the points in the narrow (P2 and P3) or wide (P7 and P8) section were
 230 used to include a sufficient number of measurement points in the determination of the median,
 231 e.g. for outer location P1:

$$\frac{|median(\bar{U}_{j-1,P2}, \bar{U}_{j,P2}, \bar{U}_{j+1,P2}, \bar{U}_{j-1,P3}, \bar{U}_{j,P3}, \bar{U}_{j+1,P3}) - \bar{U}_{j,P1}|}{\bar{U}_{j,P1}} \cdot 100 > 40 \quad (7)$$

232 Near the bed, larger changes in \bar{U} and $RMS(u')$ are likely and therefore, the lowest measurement
 233 elevation was excluded from this outlier analysis. To make sure no outliers are left near the bed,
 234 the lowest measurement elevation was compared only to the nearest upstream and downstream
 235 locations at the lowest measurement elevation. The second stage of data cleaning, discarded as
 236 little as 1% and up to 7% of the datapoints from an experimental dataset. To maintain enough
 237 datapoints over the depth, the full measurement location (P1-P9) was deemed invalid if >50% of
 238 the data was classified as outliers over the full flow depth. The bed height, z_b , was defined as the
 239 lowest valid measurement elevation. To compare the same elevation in different flows, the flows
 240 are plotted against normalized height adjusted to the deposit level.

$$\tilde{z} = (z - z_b)/h_0 \quad (8)$$

241 Following Wan (1982), the dynamic viscosity, η [$N/(s/m^2)$], of the suspensions was estimated
 242 from the measured suspended sediment concentration:

$$\eta = 0.001 + 0.206 \left(\frac{C}{100} \right)^{1.68} \quad (9)$$

243 Then, the Reynolds number was calculated as:

$$Re = \frac{\bar{U}h_0}{\nu_e} \quad (9)$$

244 where, the effective viscosity of the suspension, ν_e , was calculated from the ratio of dynamic
 245 viscosity over the density of the clay suspension, ρ_m :

$$\nu_e = \eta/\rho_m \quad (10)$$

246 The identified adaptation length, L , and time scales, T , are calculated in dimensionless form with
 247 the standing water depth as characteristic length scale and the discharge as characteristic time
 248 scale, for which the velocity at P2 is representative.

$$L = l/h_0 [-] \quad (11)$$

$$T = t \cdot h_0/U_{P2} [-] \quad (12)$$

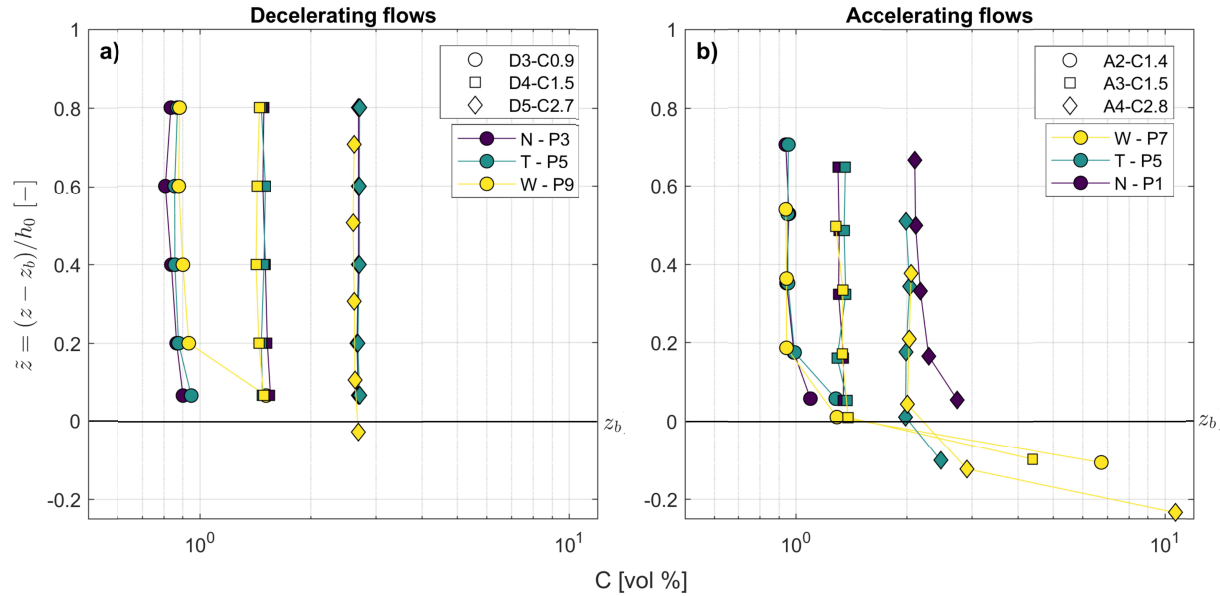
249 where l is the identified adaptation length in the flume and t the identified adaptation time in the
 250 flume.

251 3 Results

252 The results section provides an overview of the collected measurements. This includes
 253 suspended sediment concentrations (Section 3.1) and streamwise velocity and turbulence
 254 intensity profiles along the flume for decelerating flows (Section 3.2) and accelerating flows
 255 (Section 3.3).

256 3.1 Clay concentration

257 The suspended sediment concentrations for the decelerating flows were nearly uniform over the
 258 flow depth (Fig. 3a). The exception is run D3-C0.9, which contained a higher clay concentration
 259 at the lowest sampling point in the wide section (P9) of the flume. This may be explained as D3-
 260 C0.9 has the slowest recorded velocity at P9, of the decelerating flows, and thus the greatest
 261 likelihood for deposition from suspension of the cohesive sediment (Fig. 5a). The suspended
 262 sediment concentrations for the accelerating flows were non-uniform over the flow depth, with
 263 higher near-bed sediment concentrations, particularly in the wide section of the flume (Fig. 3b).
 264 These higher concentrations were in the deposit level of the flows ($\tilde{z} < 0$).
 265



266
 267 Figure 3. Vertical profiles of volumetric sediment concentration against normalized bed height
 268 adjusted to the deposit (eq 8) for the a) decelerating and b) accelerating clay-laden flows. The
 269 measurement locations are indicated in the order of the flow direction, where N, T and W denote
 270 narrow, tapering, and wide sections, respectively.

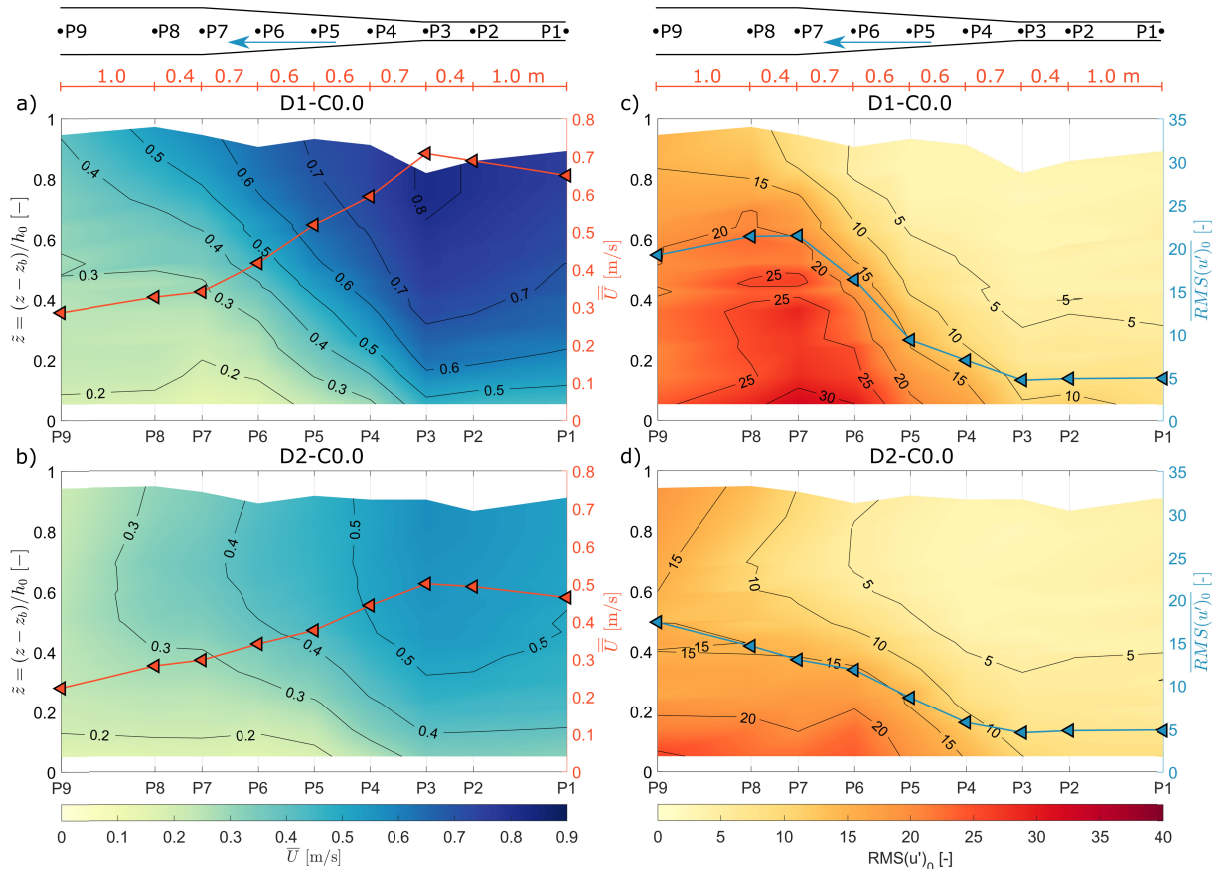
271 3.2 Decelerating flows

272 3.2.1 Clear water flows

273 Figure 4a shows the time-averaged streamwise velocity profiles (\bar{U}) and the depth-averaged
 274 velocity magnitudes (\bar{U}) along the flume for the decelerating clear-water flow D1-C0.0.
 275 Upstream, in the narrow section of the flume (P1 to P3; Fig. 2b), the depth-averaged velocity
 276 shows that the flow is nearly uniform. The velocity decreases progressively as the width of the
 277 flume increases (P4 to P6) and continues to decrease more gradually in the wide section of the
 278 flume (P7 to P9). At the end of the flume (P9), uniform conditions are established in the lower
 279 half of the flow, but they are not fully established in the upper half. Figure 4b shows the
 280 velocities along the flume for the lower-discharge decelerating flow D2-C0.0 (Table 1). The
 281 depth-averaged velocities show a comparable pattern to flow D1-C0.0 (Fig. 4a, b).

282
 283 Figures 4c and 4d show the time-averaged streamwise turbulence intensity profiles ($RMS(u')_0$)
 284 and the depth-averaged turbulence intensities ($\overline{RMS(u')_0}$) along the flume for D1-C0.0 and D2-
 285 C0.0, respectively. The depth-averaged turbulence intensity values of both flows are nearly
 286 uniform in the narrow section (P1 to P3). The turbulence intensities decrease away from the bed
 287 in the narrow section (Fig 4c, d). As the velocity decreases in the widening section (P4 to P6),
 288 turbulence intensity increases near the bed, while also progressively increasing upwards in the
 289 flow downstream. In both flows, this results in an increase in vertical gradient of turbulence
 290 intensity in the widening section followed by a decrease in the vertical gradient in the wide
 291 section. The depth-averaged turbulence intensity at P9 is 4.0 times higher than at P2 for D1-C0.0
 292 (Fig. 4c) and 3.7 times higher for D2-C0.0 (Fig. 4d), despite the decrease in velocity. Similar
 293 increases in turbulence intensity have been observed before in clear water decelerating flows

294 (Kironota and Graf, 1995; Qingyang, 2009). Towards the end of the wide section, at P9, the
 295 turbulence intensities remain non-uniform, suggesting that the length of the flume is insufficient
 296 to establish equilibrium after the widening section.
 297



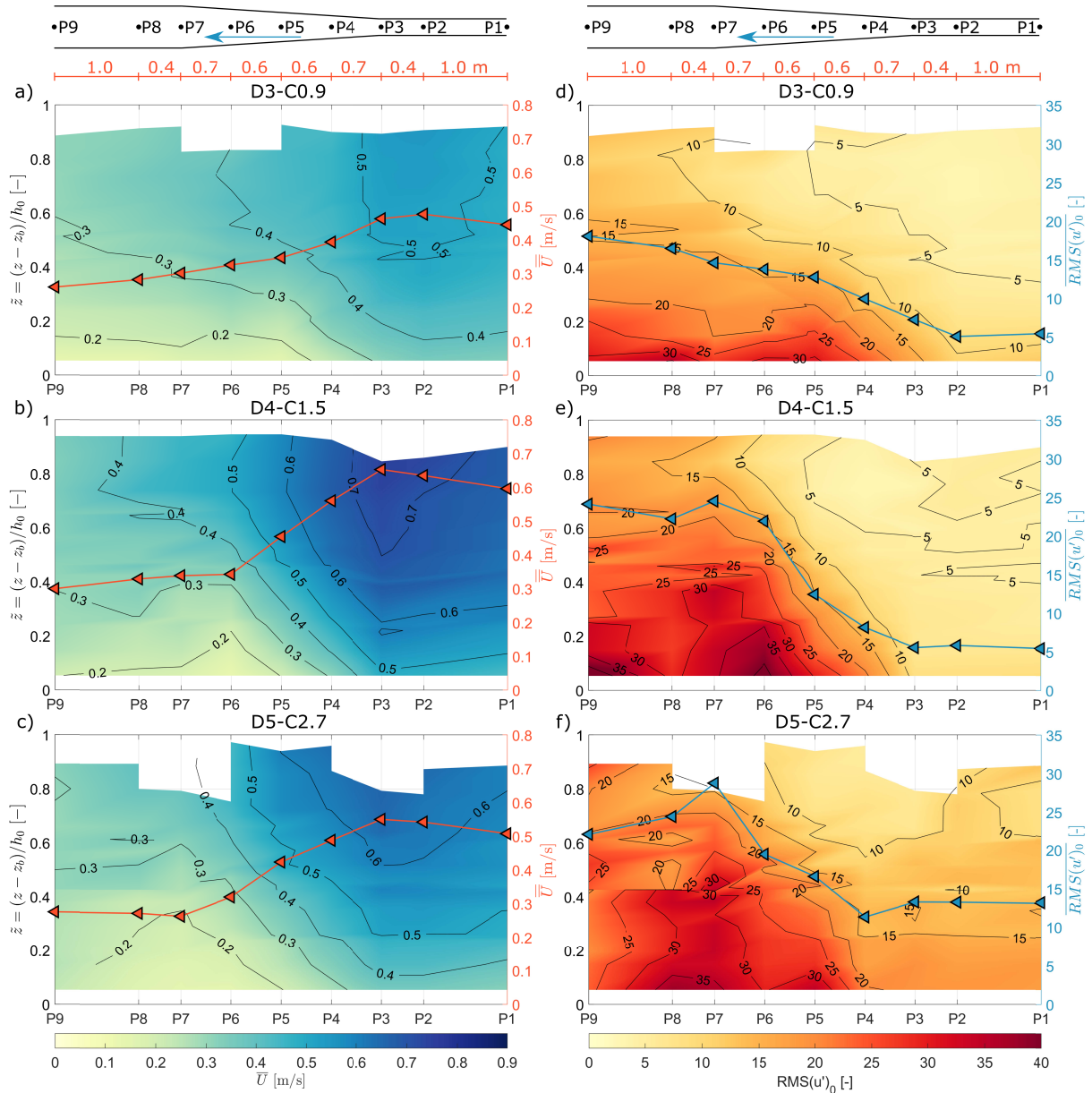
298
 299 Figure 4. Depth-averaged velocity magnitudes (\bar{U}) and time-averaged streamwise velocity
 300 profiles (\bar{U}) along the flume for the decelerating clear water flows a) D1-C0.0 and b) D2-C0.0.
 301 Depth-averaged turbulence intensities ($\overline{RMS(u')_0}$) and time-averaged streamwise turbulence
 302 intensity profiles ($RMS(u')_0$) along the flume for flows c) D1-C0.0 and d) D2-C0.0.

303 3.2.2 Clay-laden flows

304 Figures 5a, 5b and 5c show the time-averaged streamwise velocity profiles (\bar{U}) and the depth-
 305 averaged velocity magnitudes (\bar{U}) along the flume for the clay-laden decelerating flows D3-C0.9,
 306 D4-C1.5 and D5-C2.7, respectively. Figures 5d, 5e and 5f show the time-averaged streamwise
 307 turbulence intensity profiles ($RMS(u')_0$) and the depth-averaged turbulence intensities
 308 ($\overline{RMS(u')_0}$) along the flume for the same flows. In the narrow section (P1 to P3), the depth-
 309 averaged velocities are nearly uniform for each decelerating clay-laden flow. The depth-averaged
 310 velocities for each flow decrease along the widening section similarly, albeit with a slightly
 311 higher rate of decrease for flow D4-C1.5. In the wide section (P7 to P9), the depth-averaged
 312 velocities are lowest and nearly uniform.
 313

314 The depth-averaged turbulence intensity values are nearly uniform in the narrow section (P1 to
 315 P3) (Figs 5d, 5e and 5f); the turbulence intensities decrease away from the bed. As the velocity

316 decreases in the widening section (P4 to P6), the turbulence intensity increases, initially near the
317 bed, and then progressively higher in the flow downstream. This results in an increase in vertical
318 gradient of turbulence intensity in the widening section followed by a decrease in vertical
319 gradient into the wide section. Towards the end of the wide section, at P9, the turbulence
320 intensity shows a steep vertical gradient for flows D3-C0.9 and D4-C1.5. The turbulence
321 intensity for flow D5-C2.7 remains high between P7 and P9. Despite the decrease in velocity, the
322 depth-averaged turbulence intensity at P9 is 3.6 times higher than at P2 for D3-C0.9, 4.3 times
323 higher for D4-C1.5 and 1.8 times higher for D5-C2.7. Towards the end of the wide section, at
324 P9, the turbulence intensities remain non-uniform, suggesting that the length of the flume is
325 insufficient to establish equilibrium after the widening section. Despite, both the clear water and
326 clay-laden decelerating flows not reaching equilibrium flow conditions in the wide section,
327 distinct differences in patterns of increase in turbulence intensity can be identified, which
328 determines clay flow type, discussed below in Section 4.1.
329



330
 331 Figure 5. Depth-averaged velocity magnitudes (\bar{U}) and time-averaged streamwise velocity
 332 profiles (\bar{U}) along the flume for the decelerating clay-laden flows a) D3-C0.9, b) D4-C1.5 and c)
 333 D5-C2.7. Depth-averaged turbulence intensities ($\overline{RMS}(u')_0$) and time-averaged streamwise
 334 turbulence intensity profiles ($RMS(u')_0$) along the flume for flows d) D3-C0.9, e) D4-C1.5 and
 335 f) D5-C2.7.

336 3.3 Accelerating flows

337 The flow direction was reversed to achieve accelerating conditions, so the flow direction was
 338 from left to right, i.e. from P9 to P1 (cf. Fig. 2a and 2b).

339

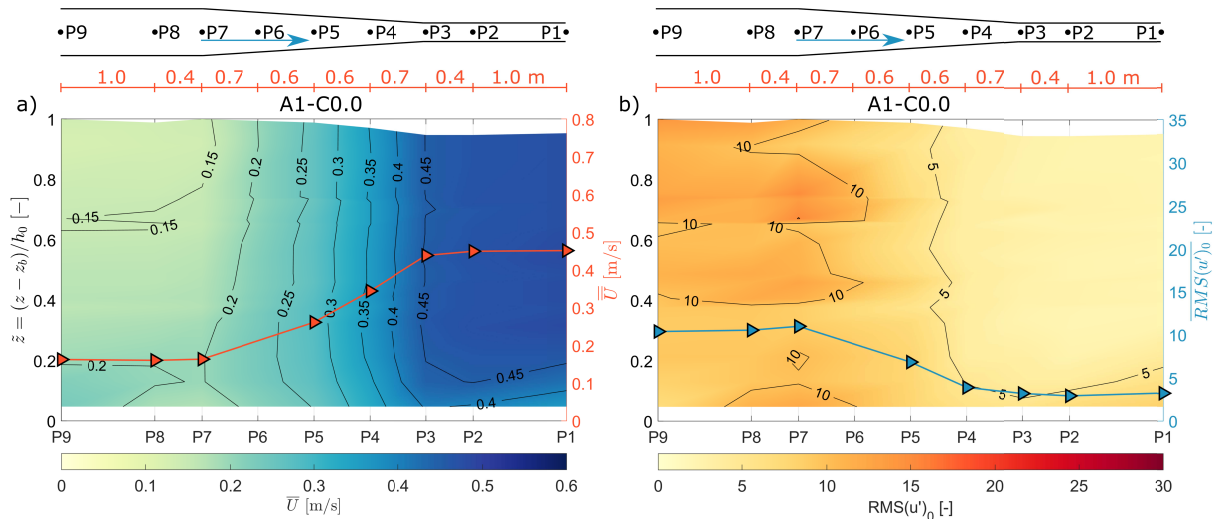
3.3.1 Clear water flows

340 Figure 6a shows the time-averaged streamwise velocity profile (\bar{U}) and the depth-averaged
 341 velocity magnitude (\bar{U}) along the flume for the accelerating clear-water flow A1-C0.0. Upstream,
 342 in the wide section of the flume (P9 to P7; Fig. 2b), the depth-averaged velocity shows that the
 343 flow is nearly uniform. The flow accelerates progressively as the width of the flume decreases
 344 (P6 to P4) and nearly uniform flow re-establishes in the narrow section (P3 to P1).

345

346 Figure 6b shows the time-averaged streamwise turbulence intensity profile ($RMS(u')_0$) and the
 347 depth-averaged turbulence intensities ($\overline{RMS(u')_0}$) along the flume for flow A1-C0.0. The depth-
 348 averaged turbulence intensity values are nearly uniform in the wide section (P9 to P7). The
 349 turbulence intensity values decrease as the velocity increases in the narrowing section (P6 to P4)
 350 and remain nearly uniform in the narrow section (P3 to P1). The depth-averaged turbulence
 351 intensity at P1 is lower by a factor of 0.3 than at P8. The velocity increases towards the narrow
 352 section, but its standard deviation ($RMS(u')$) does not rise accordingly, which results in a
 353 decrease in turbulence intensity ($RMS(u')_0$). Similar decreases in turbulence intensity have been
 354 observed before in accelerating clear water flows (Cardoso et al., 1991).

355



356

357 Figure 6. a) Depth-averaged velocity magnitudes (\bar{U}) and time-averaged streamwise velocity
 358 profiles (\bar{U}) along the flume for the accelerating clear water flow A1-C0.0. b) Depth-averaged
 359 turbulence intensities ($\overline{RMS(u')_0}$) and time-averaged streamwise turbulence intensity profiles
 360 ($RMS(u')_0$) along the flume for flow A1-C0.0.

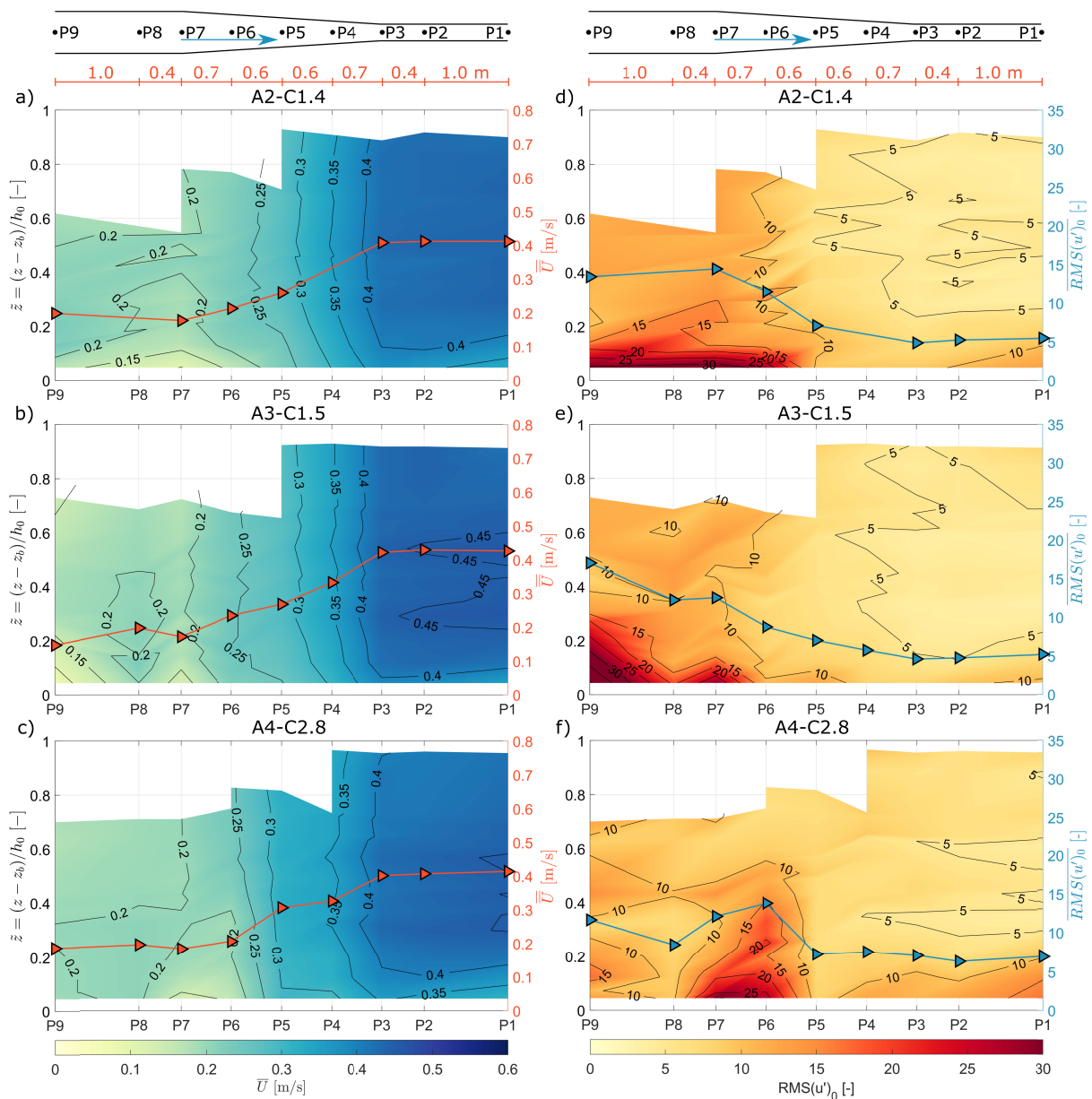
361

3.3.2 Clay-laden flows

362 Figures 7a, 7b and 7c show the time-averaged streamwise velocity profiles (\bar{U}) and the depth-
 363 averaged velocity magnitudes (\bar{U}) along the flume for the clay-laden accelerating flows A2-C1.4,
 364 A3-C1.5 and A4-C2.8, respectively. Figures 7d, 7e and 7f show the time-averaged streamwise
 365 turbulence intensity profiles ($RMS(u')_0$) and the depth-averaged turbulence intensities
 366 ($\overline{RMS(u')_0}$) along the flume for the same flows. Upstream in the wide section (P9 to P7; fig 2b),
 367 the depth-averaged velocity shows that the flow is nearly uniform. The flow accelerates
 368 progressively as the width of the flume decreases (P6 to P4) and nearly uniform flow re-
 369 establishes in the narrow section (P3 to P1).

370
 371
 372
 373
 374
 375
 376
 377
 378
 379
 380
 381
 382

In the wide section (P9 to P7), where the velocity is low, the depth-averaged turbulence intensities of all three clay flows are higher than in the narrowing and narrow sections, where the velocities are higher (Fig. 7d, 7e and 7f). Towards the base of the flow, the turbulence intensity shows a steep vertical gradient in the wide section, with especially high turbulence intensity towards the base of flows A2-C1.4 and A3-C1.5. Notably, the turbulence intensity in the bottom half of the flow at P9 and P8 in the wide section of the flume is lower for flow A4-C2.8 (Fig. 7f) than for flows A2-C1.4 (Fig 7d) and A3-C1.5 (Fig 7e). The turbulence intensity values are high around P7 for flow A4-C2.8. The depth-averaged turbulence intensity values for all three flows decrease as the velocity increases in the narrowing section (P6 to P4) and remain nearly uniform in the narrow section (P3 to P1). The depth-averaged turbulence intensity at P1 is 0.4 times the intensity at P8 for A2-C1.4, 0.4 times for A3-C1.5 and 0.8 times for A4-C2.8.



383

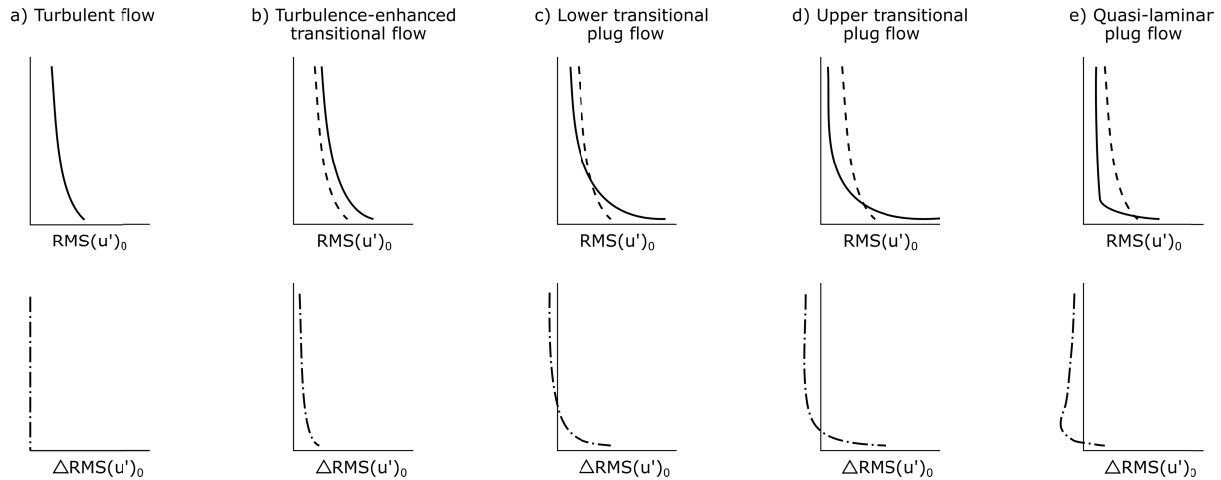
384 Figure 7. Depth-averaged velocity magnitudes (\overline{U}) and time-averaged streamwise velocity
385 profiles (\overline{U}) along the flume for the accelerating clay-laden flows a) A2-C1.4, b) A3-C1.5 and c)
386 A4-C2.8. Depth-averaged turbulence intensities ($\overline{RMS(u')_0}$) and time-averaged streamwise
387 turbulence intensity profiles ($RMS(u')_0$) along the flume for flows d) A2-C1.4, e) A3-C1.5 and
388 f) A4-C2.8.
389

390 4 Discussion

391 The discussion includes the interpretation of downstream changes in clay flow types in the
392 experimental runs (Section 4.1). Based on the distance between the different clay flow types in
393 the flume, the length scale of adaptation of clay flows is assessed in Section 4.2. The length
394 scales of decelerating and accelerating clay-laden flows are compared and further implications of
395 the present study are discussed in Section 4.3.

396 4.1 Clay flow types

397 To determine the clay flow types at the nine measurement locations along the flume initially
398 without influences of flow deceleration or acceleration, the difference in turbulence intensity is
399 assessed between clay-laden flows and clear water flows. Figure 8 shows the profiles of
400 turbulence intensity ($RMS(u')_0$) for the five clay flow types identified by Baas et al. (2009) with
401 an added dashed line indicating the turbulence intensity profile of a clear water turbulent flow.
402 Additionally, Figure 8 shows the difference profiles of turbulence intensity ($\Delta RMS(u')_0$)
403 between the five clay flow types and clear water turbulent flow. When compared with turbulent
404 clear water flow, the difference in turbulence intensity is negligible if the clay-laden flow is
405 classified as turbulent flow. Turbulence-enhanced transitional flows show higher turbulence
406 intensity over the full flow depth and thus, if compared with turbulent flow, the difference profile
407 ($\Delta RMS(u')_0$) results in positive values over the full flow depth. The plug flow formation below
408 the surface for lower transitional plug flows results in negative $\Delta RMS(u')_0$ values below the
409 surface in the difference profile. However, increased $\Delta RMS(u')_0$ values are found near the bed,
410 since lower transitional plug flow exhibits increased near-bed turbulence. With the thickening of
411 the plug flow in upper transitional plug flows, negative $\Delta RMS(u')_0$ values expand towards the
412 bed. Fully suppressed turbulence in quasi-laminar plug flows results in a negative difference
413 profile over most of the flow depth.
414



415
416 Figure 8. Upper row: schematic model of turbulence intensity profiles ($RMS(u')_0$), divided into
417 five different clay flow types after the classification scheme of Baas et al. (2009), where the
418 dashed line in b-e indicates the turbulence intensity profile for turbulent flow. Lower row:
419 schematic model of the difference in time-averaged streamwise turbulence intensity profiles
420 ($\Delta RMS(u')_0$) between clay flow types and clear water turbulent flows.
421

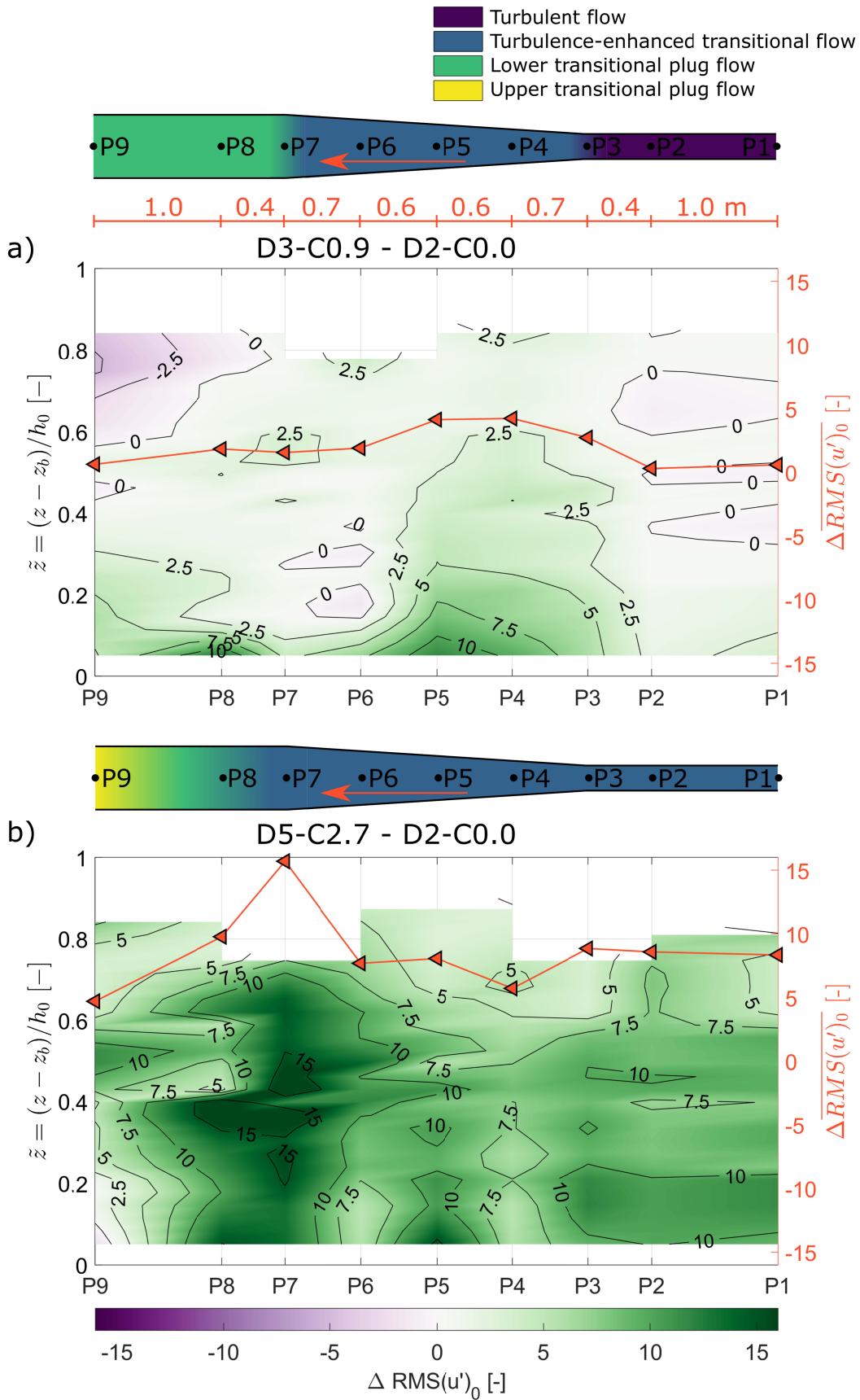
422 Figures 9a and 9b show the difference in time-averaged streamwise turbulence intensity profiles
423 ($\Delta RMS(u')_0$) and in depth-averaged turbulence intensities ($\overline{\Delta RMS(u')_0}$) along the flume for
424 decelerating flows D3-C0.9 and D5-C2.7 versus flow D2-C0.0 and Table 2 shows an overview
425 of the identified clay-flow types. Differences between the normalized turbulence intensity,
426 $RMS(u')_0$, over the normalized flow depth, \bar{z} , allows the assessment of relative influence of clay
427 concentration on non-uniform decelerating flow conditions and allows the interpretation of clay
428 flow types. Since the relative influence of clay concentration is assessed on the flow dynamics,
429 the same flow types can be identified by comparison of the decelerating clay-laden flows
430 between either clear water flows (D1-C0.0 and D2-C0.0). Here, flow D2-C0.0 is selected for the
431 comparison, because the depth-averaged velocity in the narrow section (P2) before decelerating
432 the flow is more comparable to flow D3-C0.9 and D5-C2.7 (Table 1). Upstream, in the narrow
433 section (P1 to P3; Fig. 2b), the turbulence intensity values of flow D3-C0.9 are comparable with
434 the clear-water flow D2-C0.0, i.e., the $\Delta RMS(u')_0$ values are relatively close to zero. This
435 suggests turbulent flow, unaffected by the presence of the suspended clay (Fig. 8; Table 2). As
436 the flow decelerates in the widening section (P4 to P6), the $\Delta RMS(u')_0$ values increase to 10 in
437 the lower half of the flow and to 2.5 in the upper half of the flow. This is typical of turbulence-
438 enhanced transitional flow (Fig. 8; Baas et al., 2009); under these conditions the presence of the
439 clay is inferred to cause a thickening of the viscous sublayer and the development of an internal
440 shear layer with associated enhancement of turbulence (Best and Leeder, 1993; Li and Gust,
441 2000; Baas and Best, 2002). In the wide section (P7 to P9), the $\Delta RMS(u')_0$ values remain above
442 zero in the bottom half of flow D3-C0.9 and they are zero or below zero in the top half of the
443 flow. These negative $\Delta RMS(u')_0$ values suggest the onset of plug development in flow D3-C0.9,
444 i.e., lower transitional plug flow (Fig. 8; Baas et al., 2009). Flows D3-C0.9 and D4-C1.4 show
445 comparable $\Delta RMS(u')_0$ patterns (Fig. 5d and 5e), such that the same flow types can be
446 identified.
447

448 In the narrow section (P1 to P3), the increased clay concentration in flow D5-C2.7 is inferred to
 449 cause the observed positive $\Delta RMS(u')_0$ values (Fig. 9b). This suggests that flow D5-C2.7 begins
 450 as a turbulence-enhanced transitional flow (Fig. 8; Table 2; Baas and Best, 2002). The
 451 $\Delta RMS(u')_0$ values progressively increase through the widening section and beyond, suggesting
 452 the development of stronger turbulence-enhanced transitional flow (Baas et al., 2009). While the
 453 mean velocity profile of flow D5-C2.7 appears reliable, the heterogeneous vertical pattern of
 454 $\Delta RMS(u')_0$ above a relative depth of 0.4 at position P9 (Fig. 9b) may arise from artefacts in the
 455 $RMS(u')$ measurements of this flow. This hinders a reliable inference of flow type at this
 456 location, but the decrease in $\Delta RMS(u')_0$ below the relative depth of 0.4 between P8 and P9
 457 combined with a decrease in $\Delta RMS(u')_0$ near the top of the flow between P8 and P7 may
 458 indicate a change from turbulence-enhanced transitional flow via lower transitional plug flow to
 459 upper-transitional plug flow in the wide section (P7 to P9).
 460

461 Table 2. *Identified clay flow types at the measurement positions in the flume, P9 to P1. The*
 462 *labelling of the clay flow types in the table is as follows: TF = Turbulent flow; TETF =*
 463 *Turbulence-enhanced transitional flow; LTPF = Lower transitional plug flow; UTPF = Upper*
 464 *transitional plug flow; QLPF = Quasi-laminar plug flow.*

Experimental run	Clay flow type								
	P9	P8	P7	P6	P5	P4	P3	P2	P1
<i>Decelerating flow</i>									
D3-C0.9	LTPF	LTPF	LTPF	TETF	TETF	TETF	TF	TF	TF
D5-C2.7	UTPF	LTPF	TETF	TETF	TETF	TETF	TETF	TETF	TETF
<i>Accelerating flow</i>									
A2-C1.4	LTPF	LFTP	LTPF	LTPF	TETF	TETF	TETF	TETF	TETF
A4-C2.8	UTPF	UTPF	LTPF	LTPF	LTPF	TETF	TETF	TETF	TETF

465



467 Figure 9. Difference in depth-averaged turbulence intensities ($\overline{\Delta RMS(u')_0}$) and time-averaged
 468 streamwise turbulence intensity profiles ($\Delta RMS(u')_0$) along the flume for decelerating flows a)
 469 D3-C0.9 minus D2-C0.0 and b) D5-C2.7 minus D2-C0.0.

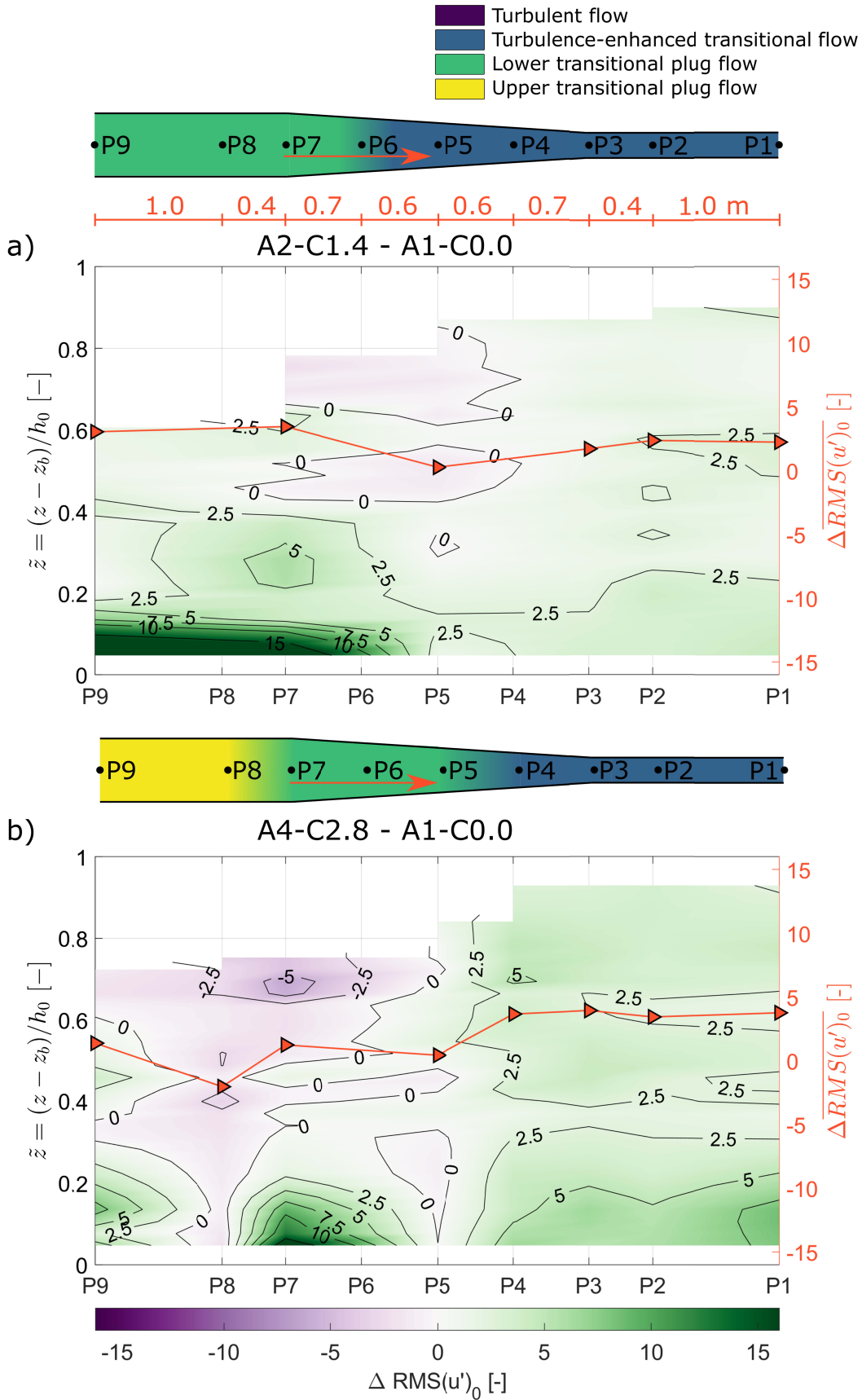
470

471 Figures 10a and 10b show the difference in time-averaged streamwise turbulence intensity
 472 profiles ($\Delta RMS(u')_0$) and in depth-averaged turbulence intensities ($\overline{\Delta RMS(u')_0}$) along the flume
 473 for accelerating flows A2-C1.4 and A4-C2.8 versus flow A1-C0.0, and Table 2 shows an
 474 overview of the identified clay-flow types. Differences between the normalized turbulence
 475 intensity, $RMS(u')_0$ over the normalized flow depth \tilde{z} allows the assessment of relative
 476 influence of clay concentration on non-uniform accelerating flow conditions and allows the
 477 interpretation of clay flow types. Upstream, in the wide section and at the start of the narrowing
 478 section (P9 to P6), $\Delta RMS(u')_0$ values are relatively close to zero in the upper half of the flow
 479 and increase downwards to 15 in the lower half of flow A2-C1.4. The high near-bed $\Delta RMS(u')_0$
 480 values, in combination with the low values in the upper half of the flow, are typical of lower
 481 transitional plug flow (Fig. 8; Baas et al., 2009). As the flow accelerates through the narrowing
 482 section (P6 to P4), the near bed $\Delta RMS(u')_0$ values progressively decrease from 10 to c. 2.5. In
 483 the narrow section (P3 to P1), the absolute turbulence intensity values of flow A2-C1.4 are low
 484 (Fig. 7d), but the $\Delta RMS(u')_0$ values are increased to around 2.5. This enhanced turbulence
 485 intensity suggests weakly turbulence-enhanced or turbulent flow (Fig. 8). Flow A3-C1.5 shows
 486 comparable turbulence intensity patterns and values (Fig. 7d and 7e) and similar flow types can
 487 be identified.

488

489 Upstream, in the wide section (P9 to P8), $\Delta RMS(u')_0$ values are up to 2.5 in the lower half of the
 490 flow and down to -2.5 in the upper half for flow A4-C2.8 (Fig. 10b). This profile suggests upper
 491 transitional plug flow, where turbulence enhancement near the bed is lower than for lower
 492 transitional plug flows (Fig. 8; cf., flow A2-C1.4 in Fig. 10a). Similar to flow A2-C1.4,
 493 $\Delta RMS(u')_0$ values of flow A4-C2.8 between P7 and P6 are relatively close to or below zero in
 494 the upper half of the flow and are as high as 15 in the lower half of the flow, suggesting lower
 495 transitional plug flow (Fig. 10b). Between P4 and P1, the depth-averaged $\overline{\Delta RMS(u')_0}$ values are
 496 between 2.5 and 5 and vertical $\Delta RMS(u')_0$ profiles are strictly positive, suggesting turbulence-
 497 enhanced transitional flow (Fig. 8).

498



500 Figure 10. Difference in depth-averaged turbulence intensities ($\overline{\Delta RMS(u')_0}$) and time-averaged
 501 streamwise turbulence intensity profiles ($\Delta RMS(u')_0$) along the flume for decelerating flows a)
 502 A2-C1.4 minus A1-C0.0 and b) A4-C2.8 minus A1-C0.0.

503 4.2 Observed adaptation length scales

504 The length scales needed by clay flows to adapt to non-uniform conditions can be estimated
 505 using the data presented in Fig. 9 and 10. The length scales are based on the identified clay-flow
 506 types (Table 2) and the distance between the measurement points at locations where a change in
 507 velocity is experienced, i.e. these estimations involve length scales downstream of the start of the
 508 widening section for the decelerating flows and the narrowing section of the accelerating flows,
 509 as well as in the wide section for the decelerating flows and in the narrow section for the
 510 accelerating flows. The adaptation length scale in the wide (decelerating flow) or narrow section
 511 (accelerating flow) is determined by the distance required to develop (nearly) uniform
 512 conditions. The adaptation length and time scales are made dimensionless using the standing
 513 water depth and the depth-averaged velocity at P2 as characteristic length and time scales (eq
 514 11,12).
 515

516 For decelerating flows, the adaptation length scales are determined at the widening section and in
 517 the wide section as the flow adapts to the change in velocity. As the flow decelerated at the start
 518 of the widening section (P3), flow D3-C0.9 changed from turbulent flow to turbulence-enhanced
 519 transitional flow, without a significant adaptation length at this position (Fig. 9a; Table 3).
 520 Throughout the wide section (P7 to P9), the flow adjusted from turbulence-enhanced transitional
 521 flow to lower transitional plug flow. Towards the end of the wide section, at P9,
 522 $\Delta RMS(u')_0$ remained non-uniform, suggesting that the length of the flume was insufficient to
 523 establish uniform conditions after the widening section (Fig. 9a). Hence, the minimum
 524 adaptation length needed to change from turbulence-enhanced flow to lower transitional plug
 525 flow was 1.4 m, the full distance between P7 and P9 (Fig. 2b). At the depth-averaged velocity of
 526 0.28 m/s in the wide section (Table 1), this adaptation length corresponds to a minimum
 527 adaptation time of 5.0 s.
 528

529 Flow D5-C2.7 started to change from a relatively weak to a stronger turbulence-enhanced
 530 transitional flow at position P4, i.e., 0.7 m into the widening section (Fig. 5f), whereas
 531 $\overline{\Delta RMS(u')_0}$ started to increase at P3 in flow D2-C0.0, i.e., at the start of the widening section
 532 (Fig. 4d). The maximum adaptation length this high-concentration clay flow needed after starting
 533 to experiencing flow widening was therefore 0.7 m (distance between P3 and P4, Fig. 2b). This
 534 is equivalent to an adaptation time of 1.4 s at a mean depth-averaged flow velocity of 0.52 m/s
 535 between P3 and P4 (Table 1). Flow D5-C2.7 changed from turbulence-enhanced transitional
 536 flow via lower transitional plug flow to upper transitional plug flow in the wide section (P7 to
 537 P9), without apparently reaching uniform flow conditions (Fig. 9b). This is equivalent to a
 538 minimum adaptation time of 5.2 s at a depth averaged flow velocity of 0.27 m/s (Table 1)
 539 through the 1.4-m long wide section (Fig. 2b).
 540

541 For accelerating flows, the adaptation length scales are determined at start of the narrowing
 542 section and in the narrow section as the flow adapts to the change in velocity. Flow A2-C1.4
 543 changed from lower-transitional plug flow at P6 to turbulence-enhanced transitional flow at P5
 544 in the narrowing section. The distance between P6 and P5 is 0.6 m and with a depth-averaged

545 velocity of 0.26 m/s, this results in an adaptation time of 2.3 s. At the start of the narrow section,
 546 P3, flow A2-C1.4 established uniform turbulence-enhanced transitional flow (Fig 10a) and show
 547 no adaptation in the narrow section itself. Hence, within the spatial resolution of the experiments,
 548 the adaptation length in the narrow section was at or close to zero.

549
 550 Flow A4-C2.8 started to change from upper transitional plug flow to lower transitional plug flow
 551 at the start of the narrowing section, at P7 and showed no signs of additional adaptation in the
 552 narrowing section (Fig. 10b) Hence, the change in clay flow type also lacked a significant delay
 553 at this location. At the start of the narrow section, P3, flow A4-C2.8 changed from lower
 554 transitional plug flow to turbulence-enhanced transitional flow. Flow A4-C2.8 established
 555 uniform turbulence-enhanced transitional flow at the start without additional adaptation in the
 556 narrow section. Hence, the change in clay flow type also lacked a significant delay at this
 557 location.

558

559 Table 3. Observed dimensional and calculated dimensionless adaptation length scales, l and L ,
 560 and time scales, t and T .

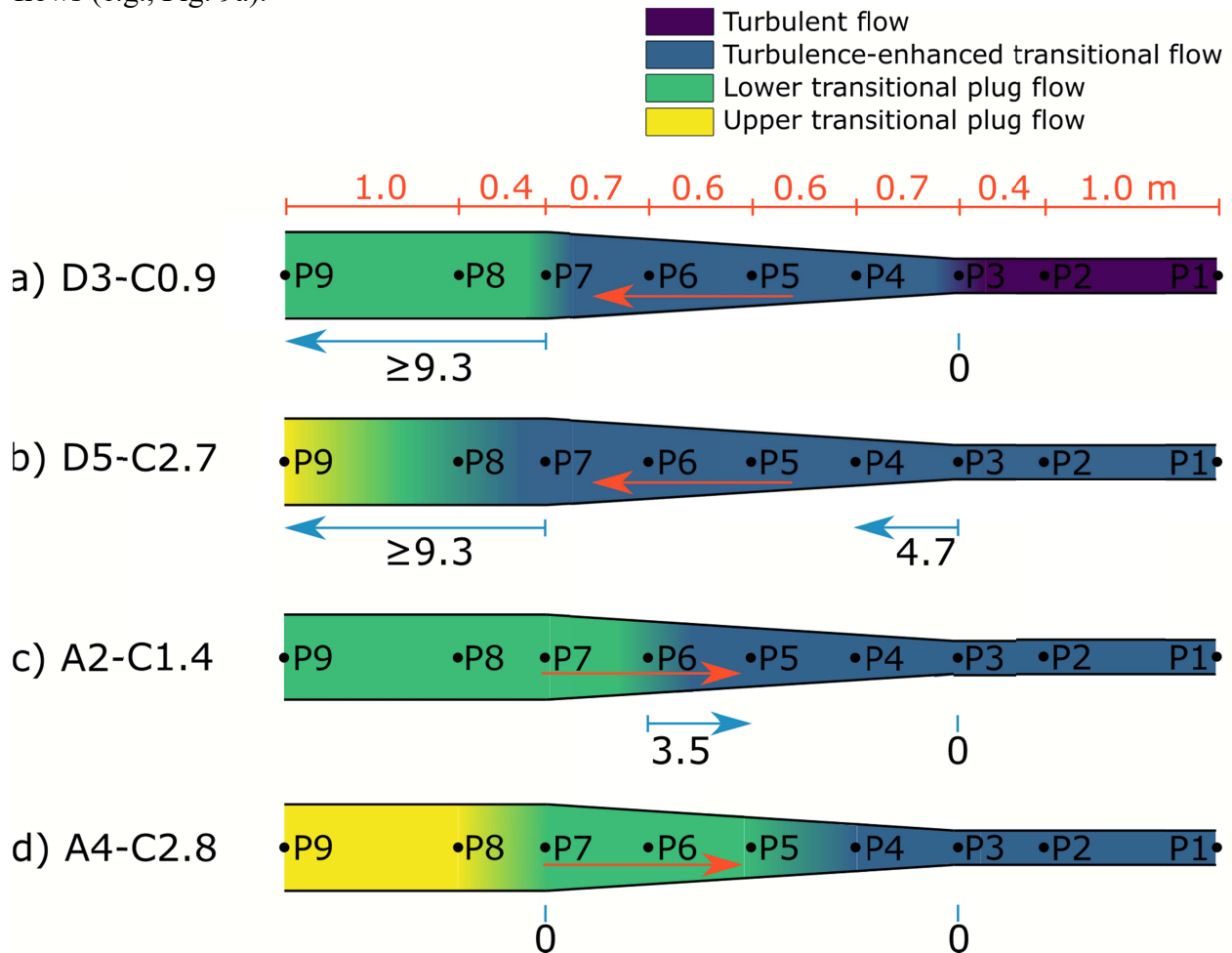
Experimental run	Location	Point(s) included in adaptation	Flow regimes	l	L	t	T
				[m]	[-]	[s]	[-]
<i>Decelerating flow</i>							
D3-C0.9	Widening section	P3	Turbulent flow to turbulence-enhanced transitional flow	0	0	0	0
	Wide section	P7 to P9	Turbulence-enhanced transitional flow to lower transitional plug flow	≥ 1.4	9.3	≥ 5.0	2.1
D5-C2.7	Widening section	P3 to P4	Weak to strong turbulence-enhanced transitional flow	0.7	4.7	1.4	0.4
	Wide section	P7 to P9	Turbulence-enhanced transitional flow to upper transitional plug flow	≥ 1.4	9.3	≥ 5.2	1.4
<i>Accelerating flow</i>							
A2-C1.4	Narrowing section	P6 to P5	Lower transitional plug flow to turbulence-enhanced transitional flow	0.6	3.5	2.3	0.9
	Narrow section	P3	Uniform turbulence-enhanced transitional flow	0	0	0	0
A4-C2.8	Narrowing section	P7	Upper transitional plug flow to lower transitional plug flow	0	0	0	0
	Narrow section	P3	Lower transitional plug flow to turbulence-enhanced transitional flow	0	0	0	0

561

562 4.3 Implications of adaptation length scales

563 Figure 11 shows an overview of the clay flow types in the experimental runs and the
 564 dimensionless adaptation length scales. The adaptation length and time scales show that the
 565 decelerating flows generally needed longer to adapt to the imposed non-uniform conditions than
 566 the accelerating flows (Fig. 11, Table 3). The largest adaptation lengths and times were at the
 567 end of the widening section in the decelerating flows, where the flows changed from turbulence-
 568 enhanced transitional flow to more cohesive lower and upper transitional plug flows. In contrast,
 569 the accelerating flows changed from the more cohesive lower transitional plug flow to
 570 turbulence-enhanced flow already in the narrowing section. These differences in adaptation
 571 length between the decelerating and accelerating flows can be explained by the fact that
 572 establishing cohesive bonds between clay particles, as in the decelerating flows, requires more
 573 time than breaking up these bonds, as in the accelerating flows.

574
 575 Stronger turbulence attenuated flow types are identified in the clay flows with higher clay
 576 concentrations. It appears to take longer to establish a pervasive network of clay bonds, as in the
 577 change from turbulence-enhanced transitional flows to lower and upper transitional plug flow at
 578 the end of the widening section in the decelerating flows, than to establish a turbulence-enhanced
 579 transitional flow from a turbulent flow by reducing the flow velocity in low-concentration clay
 580 flows (e.g., Fig. 9a).



581
 582 Figure 11. Identified clay flow types and observed dimensionless adaptation length scale, L.

583

584 The research focus here is on adaptation of flow dynamics of non-uniform clay-laden flows, but
585 the length and time scales of flow adaptation can also be reflected in the depositional product
586 (Dorrell and Hogg, 2012). Here, non-uniformity on spatial deceleration and acceleration in clay-
587 laden open-channel demonstrates that these adaptation scales in mud-rich flows fundamentally
588 differ between decelerating and accelerating regimes, due to the time required to form or break
589 cohesive bonds between particles. These results are based on streamwise velocity measurements,
590 due to the limitations of Ultrasonic Velocity Profilers, which are designed to work along a single
591 beam. Further developments in technology are needed to fully resolve the turbulent motion of
592 highly concentrated flows.

593

594 Additional research in the sedimentological record is required to determine how deposits of non-
595 uniform clay suspension flows can be recognized in fluvial, estuarine and submarine systems.
596 For example, after a sediment supply increase in a river following wild-fire related erosion
597 (Renau et al., 2007; Sankey et al., 2017; Nyman et al., 2019), flow deceleration can occur
598 following for example, a reduction in bed slope or widening of the river channel. The flow
599 deceleration reduces the turbulent forces in the flow and allows the establishment of cohesive
600 bonds between clay particles. The adaptation to stronger turbulence attenuated clay flow types
601 requires time due to the formation of clay bonds and consequently, the deposits associated with
602 the clay flow type form over the adaptation length scale downstream of the location of flow
603 deceleration. In an industrial setting such as downstream of dam flushing or venting events flow
604 acceleration can occur (Antoine et al., 2020), increasing the turbulent forces in the flow, which
605 has the potential to break up bonds between clay particles. This study shows that the adaptation
606 of the clay flow type to a stronger turbulent flow occurs more rapidly and consequently the
607 associated deposits with clay flow type occur near the location of acceleration. Additionally, the
608 different adaptation length and time scales are of particular relevance in interpreting the shape of
609 submarine deposits, such as unconfined submarine lobes (Spychala et al., 2017) and hybrid event
610 beds deposited around diapires (Davis et al., 2009; Patacci et al., 2014). It is anticipated that the
611 depositional record of decelerating flows reflects the time scales required to form interparticle
612 bonds, delaying the depositional response to the associated changes in flow conditions. For
613 accelerating flows it is anticipated that changes in deposit properties associated with bond
614 breakage occur more rapidly, such that they are more closely associated with the areas where
615 acceleration occurs.

616 **5 Conclusions**

617 This research investigated the influence of suspended cohesive clay on changing flow dynamics
618 under non-uniform flow conditions, using decelerating and accelerating open-channel flows in a
619 recirculating flume. These flows may evolve through different clay flow types with different
620 associated degrees of turbulence enhancement and attenuation depending on the clay
621 concentration and whether the flows decelerate or accelerate. Decelerating flows have a longer
622 adaptation time than accelerating flows, as establishing cohesive bonds between clay particles
623 requires more time than breaking the clay bonds. This hysteresis is more pronounced for higher-
624 concentration flows that change from the turbulence-enhanced transitional flow type to the lower
625 and upper transitional plug flow types than for lower-concentration decelerating flows that
626 change from the turbulent flow type to the turbulence-enhanced transitional flow type.
627 Differences in adaptation time likely influence the distribution and character of deposit in

628 sedimentary environments. The associated deposits with clay flow type of decelerating flows are
629 likely spread over a larger distance than of accelerating flow due to the elongated adaptation time
630 of decelerating flows.

631 **Acknowledgements**

632 This work was carried out as part of a PhD studentship, part funded through the Turbidites
633 Research Group, University of Leeds and part funded through the University of Hull. Bangor
634 University is thanked for loan of Ultrasonic Velocity Profilers for the duration of the
635 experiments. RMD is grateful for funding from NERC NE/S014535/1. Participation of RF in this
636 study has been possible thanks to The Leverhulme Trust, Leverhulme Early Career Researcher
637 Fellowship (grant ECF-2020-679) and the European Research Council under the European
638 Union's Horizon 2020 research and innovation program (grant 725955).

639 **Data Availability Statement**

640 The data collected during the physical experiments in preparation for this research is available at
641 <https://doi.org/10.5281/zenodo.6642324> (de Vet et al., 2022).

642 **References**

- 643 Ackers, J., Butler, D., Leggett, D., & May, R. (2001), Designing sewers to control sediment
644 problems. *Urban Drainage Modeling*, 818-823. doi: 10.1061/40583(275)77
645
- 646 Antoine, G., Camenen, B., Jodeau, M., Nemery, J. & Esteves, M. (2020), Downstream erosion
647 and deposition dynamics of fine suspended sediments due to dam flushing. *Journal of*
648 *Hydrology*, 585. doi: 10.1016/j.jhydrol.2020.124763
649
- 650 Baas, J.H., & Best, J.L. (2002), Turbulence modulation in clay-rich sediment-laden flows and
651 some implications for sediment deposition. *Journal of Sedimentary Research*, 72(3), 336-340.
652 doi: 10.1306/120601720336
653
- 654 Baas, J.H., Best, J.L., Peakall, J., & Wang, M. (2009), A phase diagram for turbulent,
655 transitional, and laminar clay suspension flows. *Journal of Sedimentary Research*, 79(4), 162-
656 183. doi: 10.2110/jsr.2009.025
657
- 658 Bagnold, R.A. (1954), Experiments on a gravity-free dispersion of large, solid spheres in a
659 Newtonian fluid under shear. *Proceedings of the Royal Society of London. Series A.*
660 *Mathematical and Physical Sciences*, 225(1160), 49-63. doi:10.1098/rspa.1954.0186
661
- 662 Barbero, R., Abatzoglou, J.T., Larkin, N.K., Kolden, C.A., & Stocks, B. (2015), Climate change
663 presents increased potential for very large fires in the contiguous United States. *International*
664 *Journal of Wildland Fire*, 24(7), 892-899. doi: 10.1071/WF15083
665
- 666 Best, J.L. (1988), Sediment transport and bed morphology at river channel confluences.
667 *Sedimentology*, 35(3), 481-498. doi: 10.1111/j.1365-3091.1988.tb00999.x
668

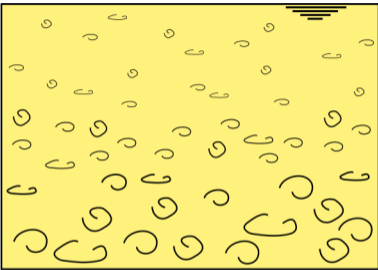
- 669 Best, J.L., & Leeder, M.R. (1993), Drag reduction in turbulent muddy seawater flows and some
670 sedimentary consequences. *Sedimentology*, 40(6), 1129-1137. doi: 10.1111/j.1365-
671 3091.1993.tb01383.x
- 672
- 673 Best, J., Bennet, S., Bridge, J., & Leeder, M.R., (1997), Turbulence modulation and particle
674 velocities over flat sand beds at low transport rates. *Journal of Hydraulic Engineering*, 123(12),
675 1118-1129. doi: 10.1061/(ASCE)0733-9429(1997)123:12(1118)
- 676
- 677 Best, J.L., Kirkbridge, A.D., & Peakall, J., (2001), Mean flow and turbulence structure of
678 sediment-laden gravity currents: new insights using ultrasonic Doppler velocity profiling, in
679 McCaffrey, W.D., Kneller, B.C., & Peakall, J., eds., Particulate Gravity Currents, *International*
680 *Association of Sedimentologists, Special Publication*, 31, 159-172. doi:
681 10.1002/9781444304275.ch12
- 682
- 683 Bilal, A., Xie, Q., & Zhai, Y., (2020), Flow, Sediment, and Morpho-Dynamics of River
684 Confluence in Tidal and Non-Tidal Environments. *Journal of Marine Science and Engineering*,
685 8(8), 591. doi: 10.3390/jmse8080591
- 686
- 687 Brenda, L., & Dunne, T., (1997), Stochastic forcing of sediment supply to channel networks
688 from landsliding and debris flow. *Water Resources Research*, 33(12), 2849-2863. doi:
689 10.1029/97WR02388
- 690
- 691 Cardoso, A.H., Graf, W.H., & Gust, G., (1991), Steady gradually accelerating flow in a smooth
692 open channel. *Journal of Hydraulic Research*, 29(4), 525-543. doi:
693 10.1080/00221689109498972
- 694
- 695 Davis, C., Haughton, P., McCaffrey, W., Scott, E., Hogg, N., & Kitching, D., (2009), Character
696 and distribution of hybrid sediment gravity flow deposits from the outer Forties Fan, Paleocene
697 Central North Sea, UKCS. *Marine and Petroleum Geology*, 26(10), 1919-1939. doi:
698 10.1016/j.marpetgeo.2009.02.015
- 699
- 700 Dorrell, R.M., & Hogg, A.J. (2012), Length and time scales of response of sediment suspension
701 to changing flow conditions. *Journal of Hydraulic Engineering*, 138(5), 430-439. doi:
702 10.1061/(ASCE)HY.1943-7900.0000532
- 703
- 704 Dorrell, R.M., Amy, L.A., Peakall, J., & McCaffrey, W.D. (2018), Particle size distribution
705 controls the threshold between net sediment erosion and deposition in suspended load dominated
706 flows. *Geophysical Research Letters*, 45(3), 1443–1452. doi: 10.1002/2017GL076489
- 707
- 708 Geertsema, M., Clague, J.J., Schwab, J.W., & Evans, S.G. (2006), An overview of recent large
709 catastrophic landslides in northern British Columbia, Canada. *Engineering Geology*, 83(1-3),
710 120–143. doi: 10.1016/j.enggeo.2005.06.028
- 711
- 712 Kironoto, B.A., & Graf, W.H. (1995), Turbulence characteristics in rough non-uniform open-
713 channel flow. *Proceedings of the institute of civil engineers water maritime and energy*, 112(4),
714 336-348. doi: 10.1680/iwtme.1995.28114

- 715
716 Li, M.Z., & Gust, G. (2000), Boundary layer dynamics and drag reduction in flows of high
717 cohesive sediment suspensions. *Sedimentology*, 47(1), 71-86. doi: 10.1046/j.1365-
718 3091.2000.00277.x
- 719
720 Mehta, A. J., McAnally Jr, W. H., Hayter, E. J., Teeter, A. M., Schoellhamer, D., Heltzel, S. B.,
721 & Carey, W. P. (1989), Cohesive sediment transport. II: Application. *Journal of Hydraulic*
722 *Engineering*, 115(8), 1094-1112. doi: 10.1061/(ASCE)0733-9429(1989)115:8(1094)
- 723
724 Moody, J. A., Shakesby, R. A., Robichaud, P. R., Cannon, S. H., & Martin, D. A. (2013),
725 Current research issues related to post-wildfire runoff and erosion processes. *Earth-Science*
726 *Reviews*, 122, 10-37. doi: 10.1016/j.earscirev.2013.03.004
- 727
728 Murphy, S.F., Writer, J.H., McClesley, R.B., & Martin, D.A. (2015), The role of precipitation
729 type, intensity, and spatial distribution in source water quality after wildfire. *Environmental*
730 *Research Letters*, 10(8). doi: 10.1088/1748-9326/10/8/084007
- 731
732 Nezu, I., & Nakagawa, H. (1993), *Turbulence in Open-Channel Flows*. Delft Hydraulics,
733 International Association for Hydraulic Research, Monograph.
- 734
735 Nyman, P., Box, W.A.C., Stout, J.C., Sheridan, G.J., Keestra, S.D., Lane, P.N.J., & Langhans,
736 C. (2019), Debris-flow-dominated sediment transport through a channel network after wildfire.
737 *Earth Surfaces Processes and Landforms*, 45(5), 115-1167. doi: 10.1002/esp.4785
- 738
739 Van Olphen, H. (1977), *An introduction to Clay Colloid Chemistry*. 2nd Edition: London, John
740 Wiley & Sons.
- 741
742 Patacci, M., Haughton, P.D.W., & McCaffrey, W.D. (2014), Rheological Complexity In
743 Sediment Gravity Flows To Decelerate Against A Confining Slope, Braux, SE France. *Journal of*
744 *Sedimentary Research*, 84(4), 270-277. doi: 10.2110/jsr.2014.26
- 745
746 Partheniades, E. (1965). Erosion and deposition of cohesive soils. *Journal of the Hydraulics*
747 *Division*, 91(1), 105-139. doi: 10.1061/JYCEAJ.0001165
- 748
749 Partheniades, E. (2009), *Cohesive sediment in open channels*. Butterworth-Heinemann,
750 Burlington (MA)
- 751
752 Qingyang, S. (2009), Velocity distribution and wake-law in gradually decelerating flows.
753 *Journal of Hydraulic Research*, 47(2), 177-184. doi: 10.3826/jhr.2009.3254
- 754
755 Reneau, S.L., Katzman, D., Kuyumjian, G.A., Lavine, A., & Malmon, D.V. (2007), Sediment
756 delivery after a wildfire. *Geology*, 35(2), 151-154. doi: 10.1130/G23288A.1
- 757
758 Rengers, F.K., McGuire, L.A., Oakley, N.S., Kean, J.W., Staley, D.M., & Tang, H. (2020),
759 Landslides after wildfire: initiation, magnitude, and mobility. *Landslides*, 17, 2631-2641. doi:
760 10.1007/s10346-020-01506-3

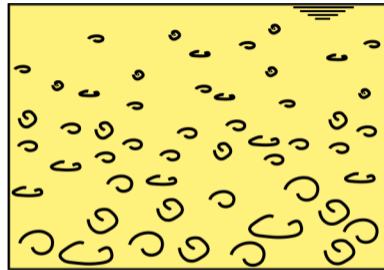
- 761
762 Sankey, J.B., Kreitler, J., Hawbaker, T.J., McVay, J.L., Miller, M.E., Mueller, E.R., Vaillant,
763 N.M., Lowe, S.E., & Sankey, T.T. (2017), Climate, wildfire, and erosion ensemble foretells
764 more sediment in western USA watersheds. *Geophysical Research Letters*, 44(17), 8884-8892.
765 doi: 10.1002/2017GL073979
- 766
767 Smith, H.G., Sheridan, G.J., Lane, P.N.J., Nyman, P., & Haydon, S. (2011), Wildfire effects on
768 water quality in forest catchments: A review with implications for water supply. *Journal of*
769 *Hydrology*, 396(1-2), 170-192. doi: 10.1016/j.jhydrol.2010.10.043
- 770
771 Spychala, Y.T., Hodgson, D.M., Prelat, A., Kane, I.A., Flint, S.S., & Mountney, N.P. (2017),
772 Frontal and Lateral Submarine Lobe Fringes: Comparing Sedimentary Facies, Architecture and
773 Flow Processes. *Journal of Sedimentary Research*, 87(1), 75-96. doi: 10.2110/jsr.2017.2
- 774
775 Swanson, F.J. (1981), Fire and geomorphic processes: in Mooney, H.A., et al., eds., Fire
776 Regimes and Ecosystem Properties: U.S. Department of Agriculture Forest Service General
777 Technical Report WO-26, 401-444
- 778
779 Takeda, Y. (1991), Development of an ultrasound velocity profile monitor. *Nuclear Engineering*
780 *and Design*, 126(2), 277-284. doi: 10.1016/0029-5493(91)90117-Z
- 781
782 Talling, P.J., Masson, D.G., Sumner, E.J., & Malgesini, G. (2012), Subaqueous sediment density
783 flows: Depositional processes and deposit types. *Sedimentology*, 59(7), 1937-2003. doi:
784 10.1111/j.1365-3091.2012.01353.x
- 785
786 Wan, Z. (1982), Bed material movement in hyperconcentrated flows, Serie paper 31, Institute of
787 Hydrodynamics and Hydraulic Engineering, Technical University of Denmark.
- 788
789 Wan, Z., & Wang, Z. (1994), *Hyperconcentrated flow*. CRC Press.
- 790
791 Wang, Z., & Larsen, P. (1994), Turbulence structure of flows of water and clay suspensions
792 with bedload. *Journal of Hydraulic Engineering*, 120(5), 577-600. doi: 10.1061/(ASCE)0733-
793 9429(1994)120:5(577)
- 794
795 Whitehouse, R. J. S., Soulsby, R. L., Roberts, W., & Mitchener, H. J. (2000). *Dynamics of*
796 *estuarine muds*. Technical Report. Thomas Telford.
- 797
798 Winterwerp, J.C. & van Kesteren, W.G.M. (2004), *Introduction to the Physics of Cohesive*
799 *Sediment in the Marine Environment*. Oxford, U.K, Elsevier, Developments in Sedimentology
800 46.
- 801

Figure1.

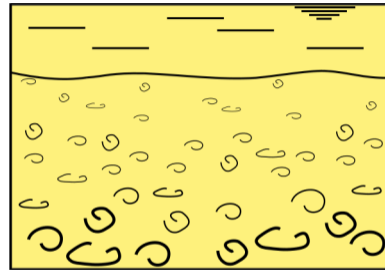
Turbulent flow



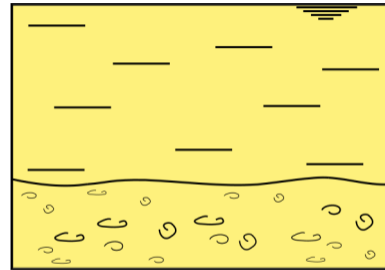
Turbulence-enhanced transitional flow



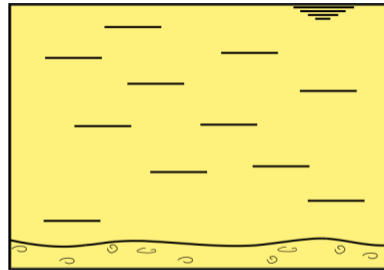
Lower transitional plug flow



Upper transitional plug flow



Quasi-laminar plug flow



Increasing clay concentration



Increasing flow velocity



Turbulent forces

Cohesive forces



Figure2.

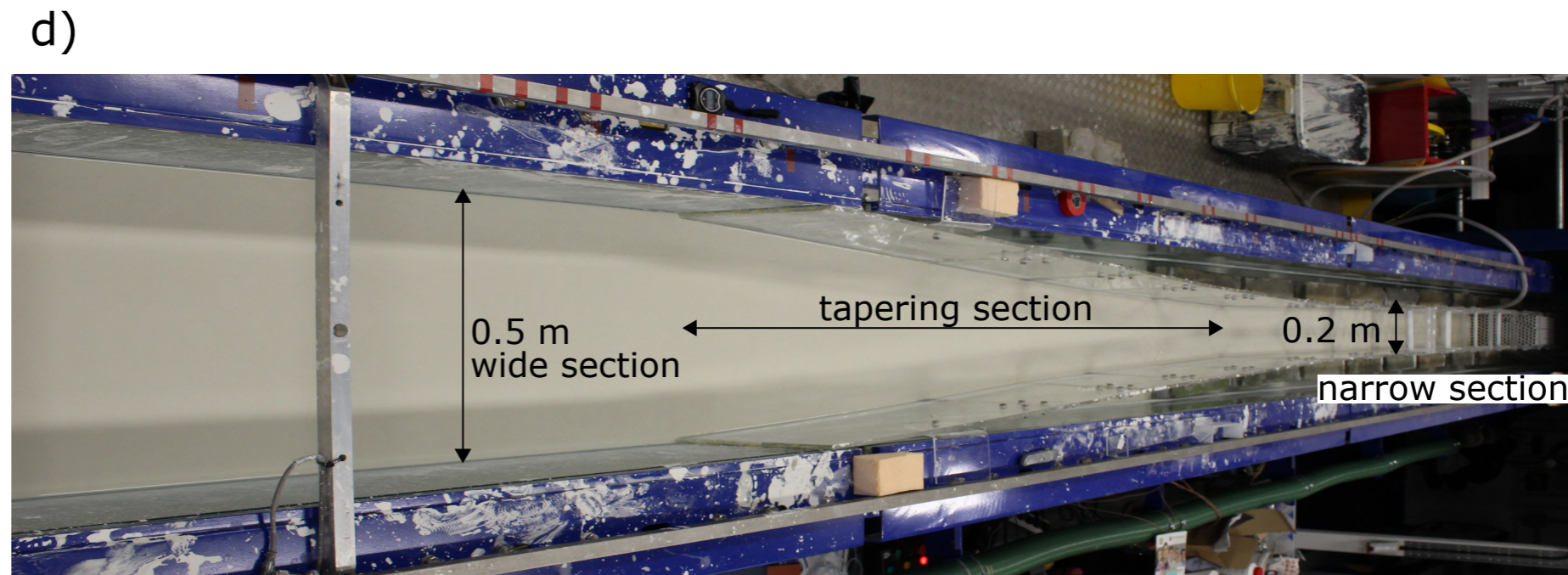
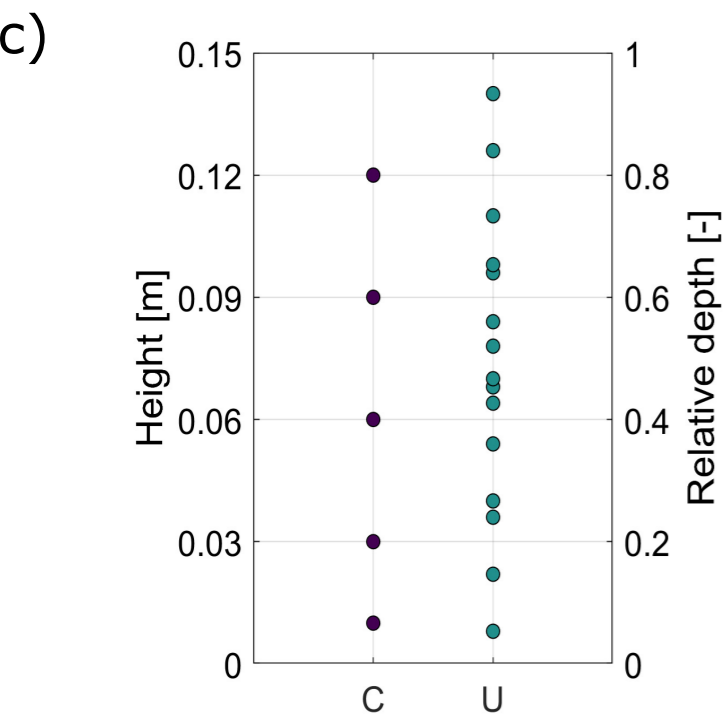
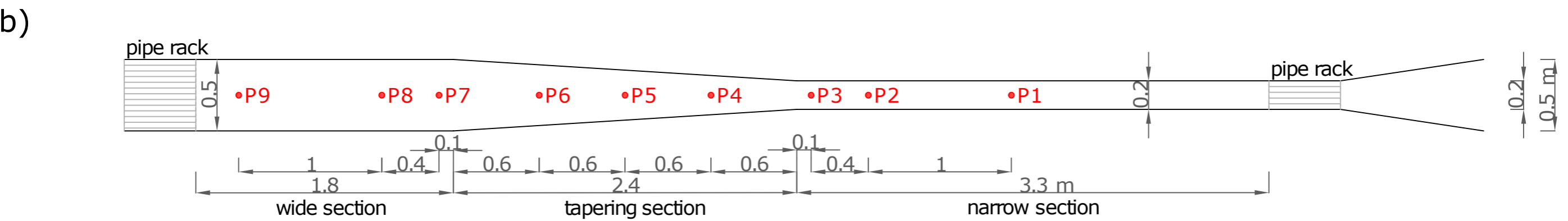
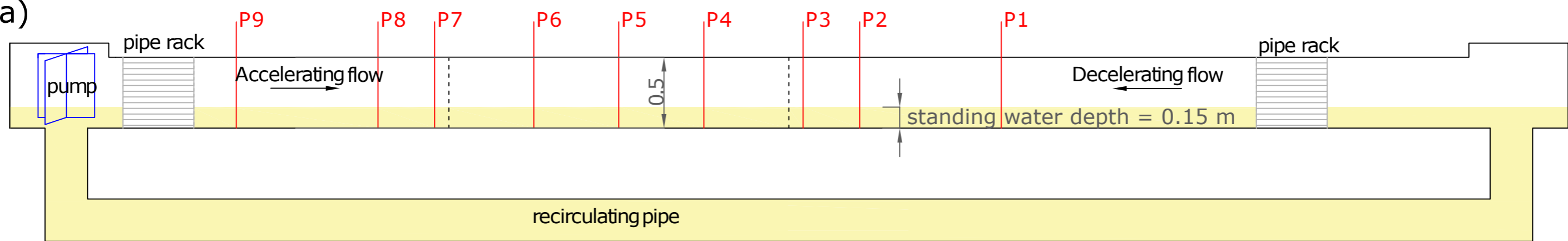


Figure3.

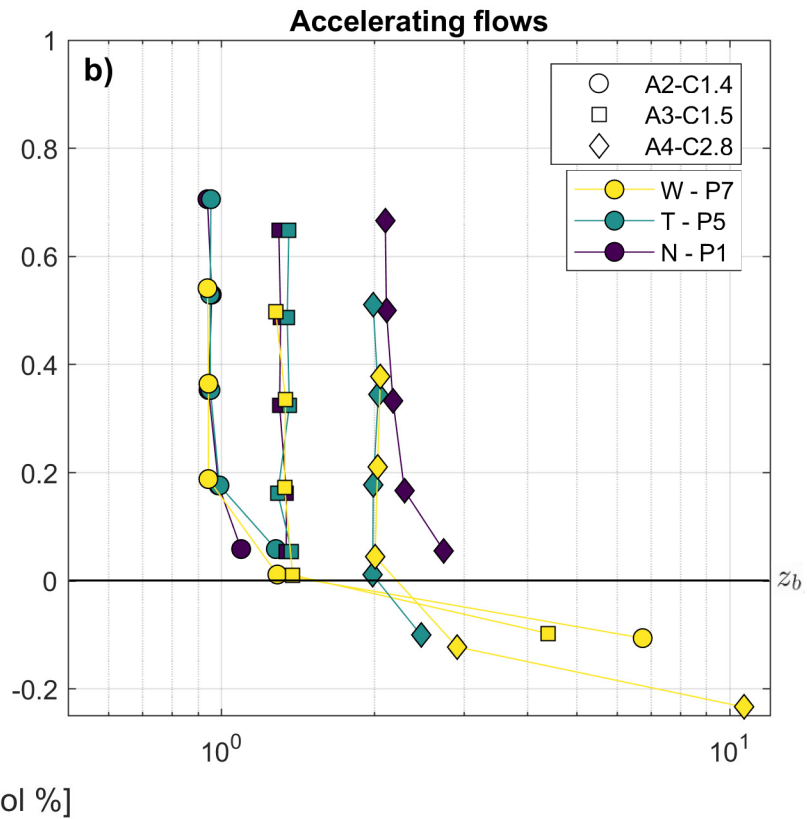
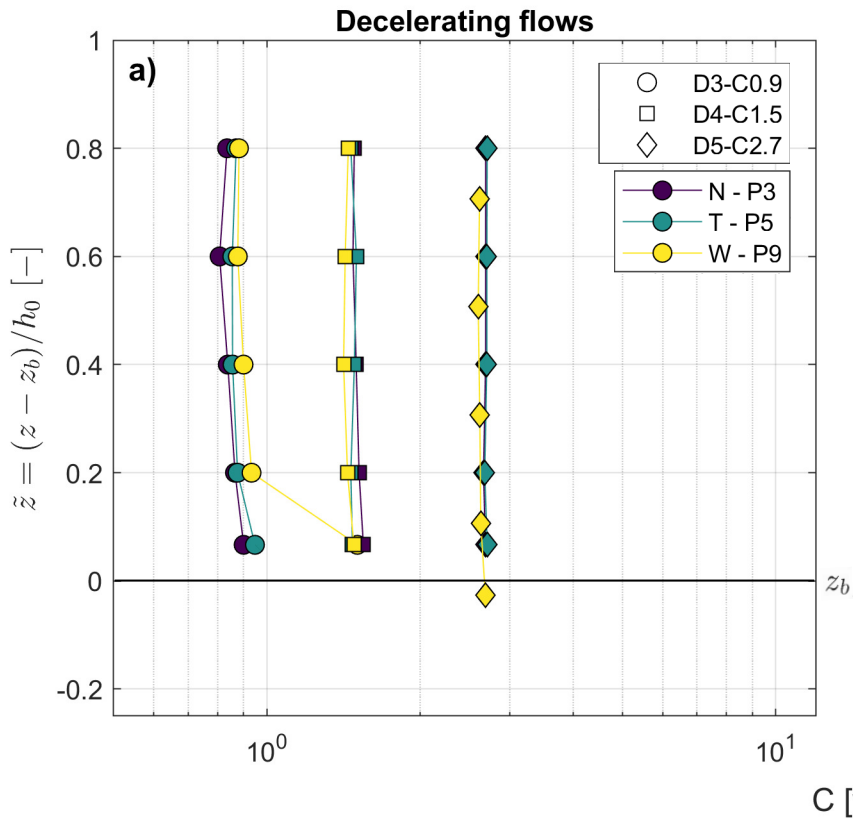


Figure4.

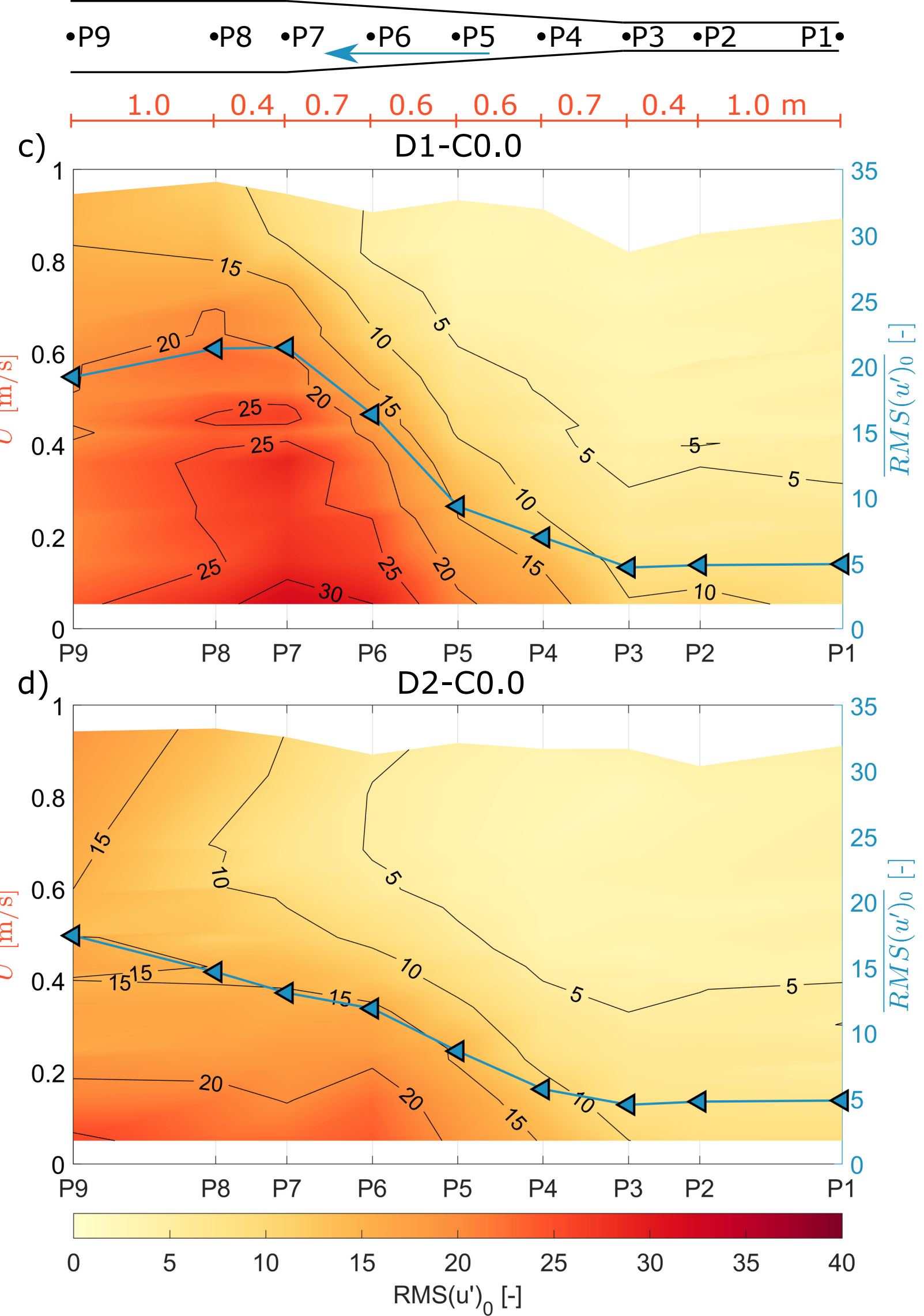
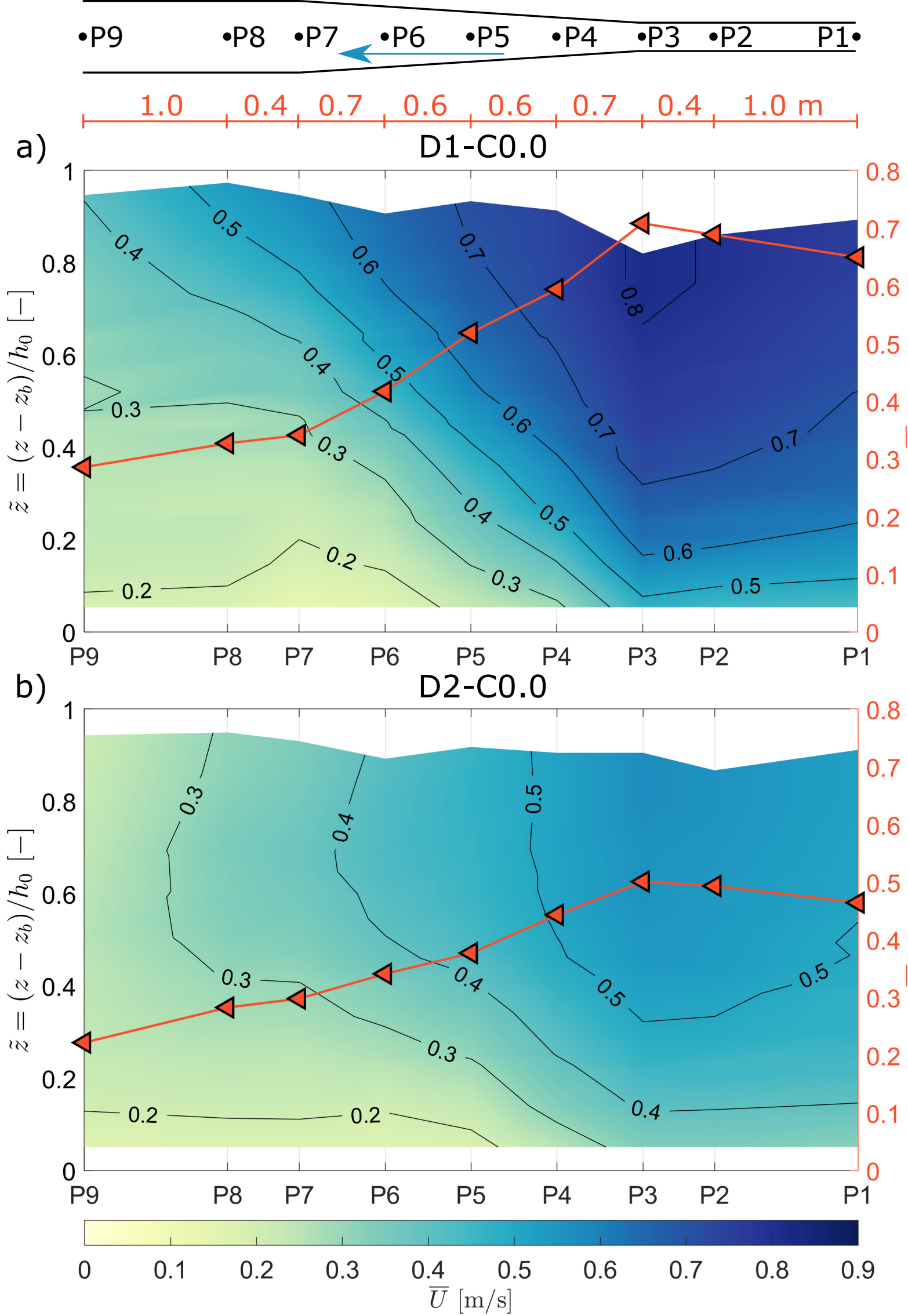


Figure 5.

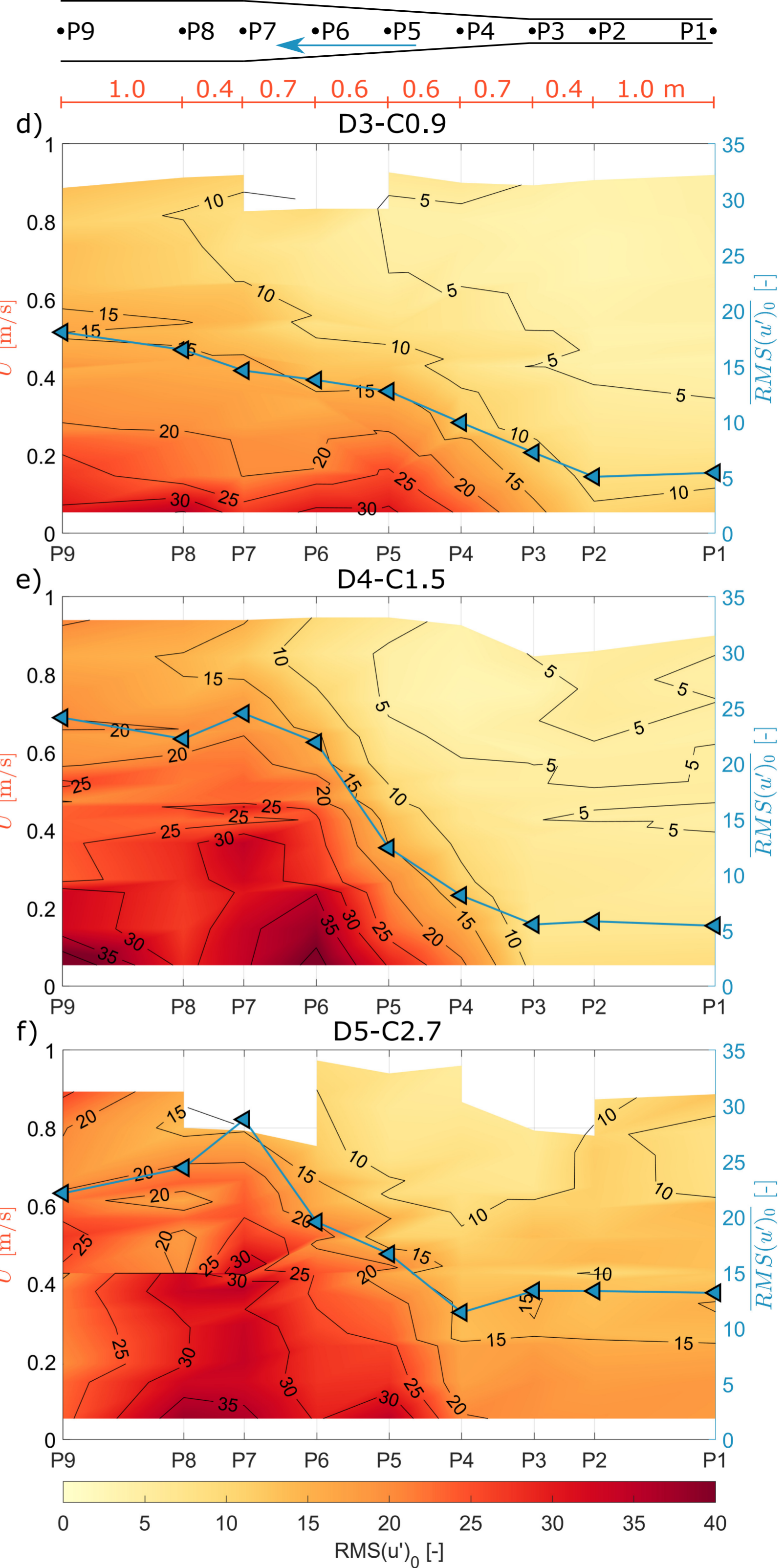
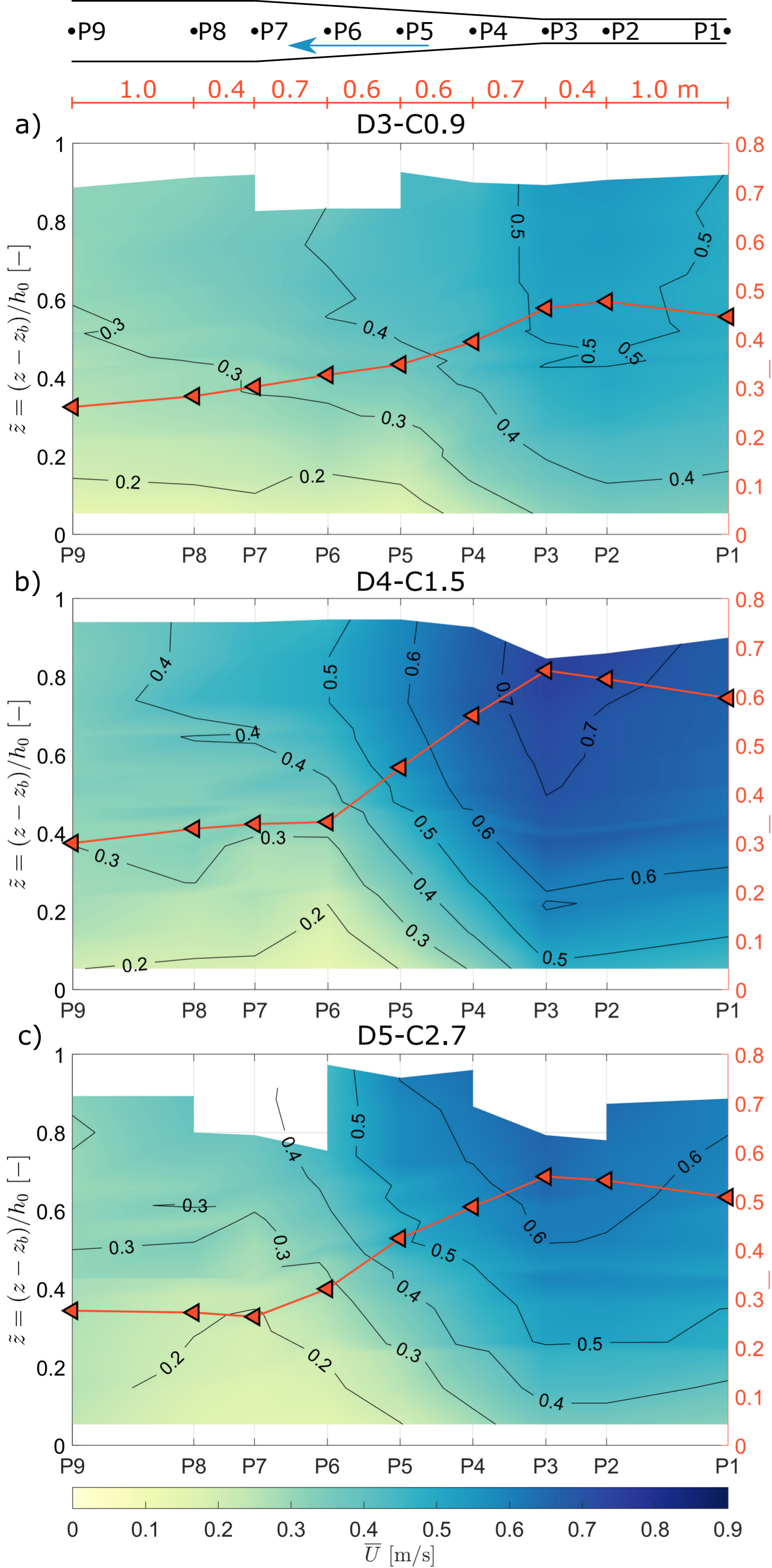


Figure6.

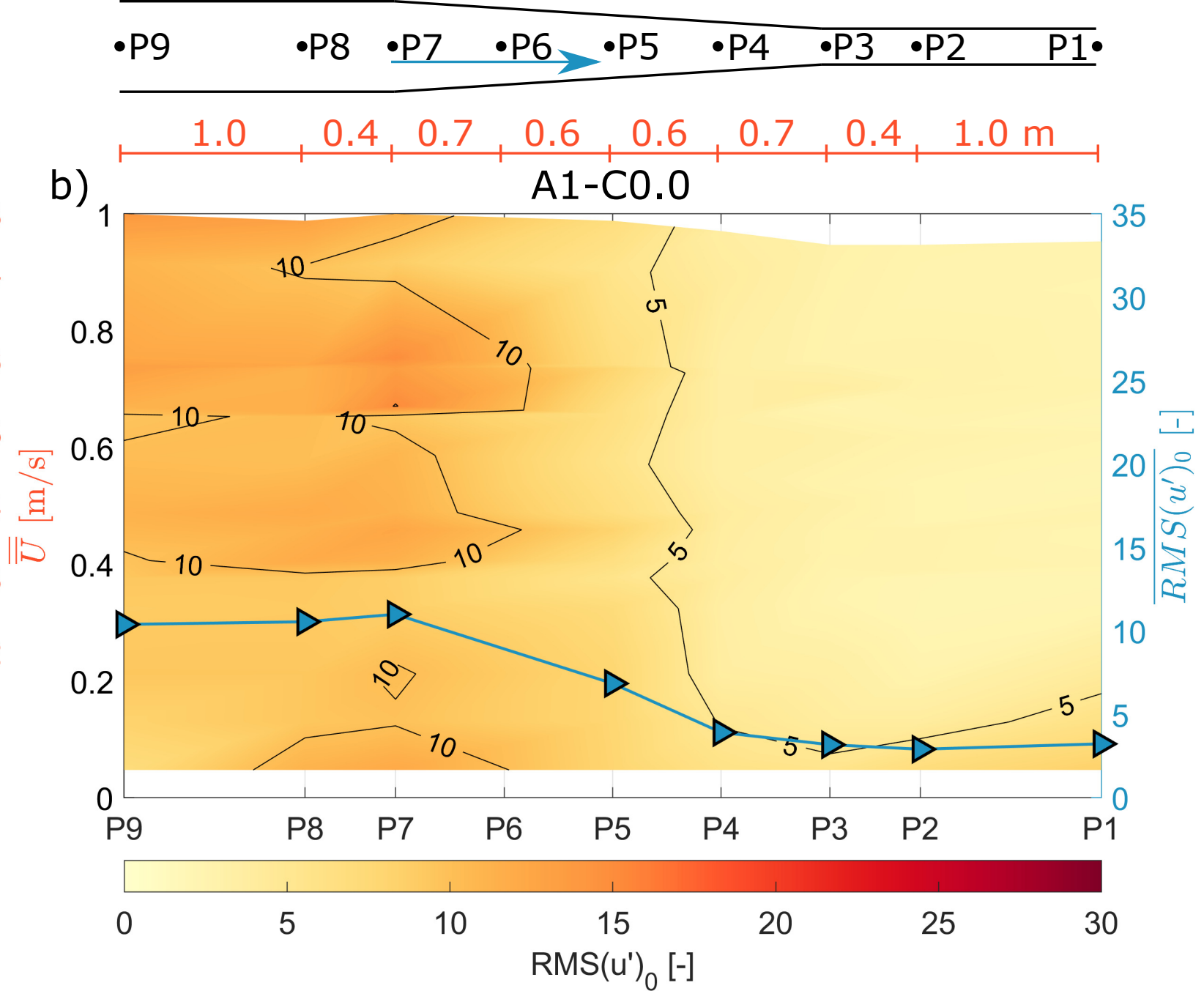
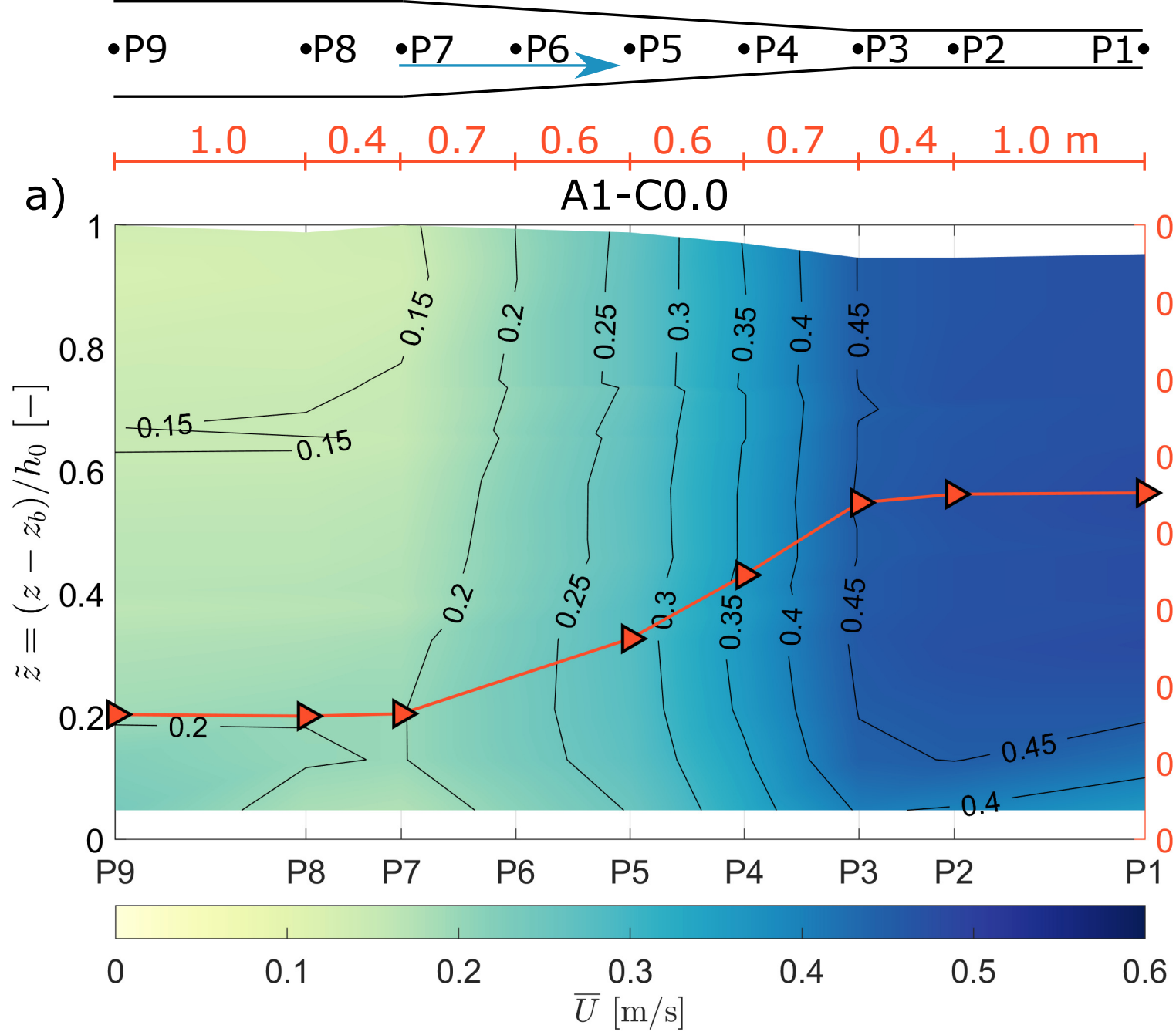


Figure7.

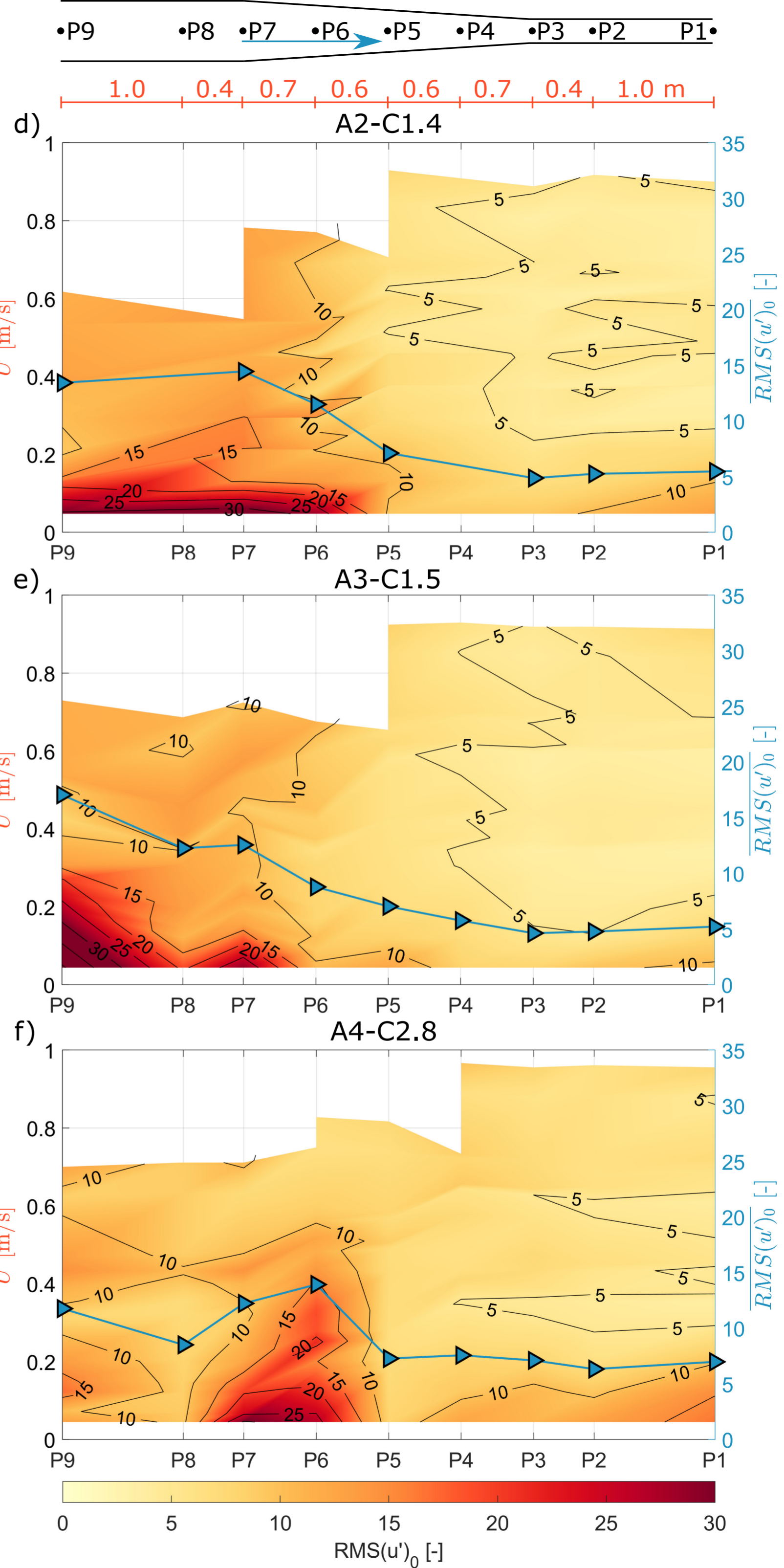
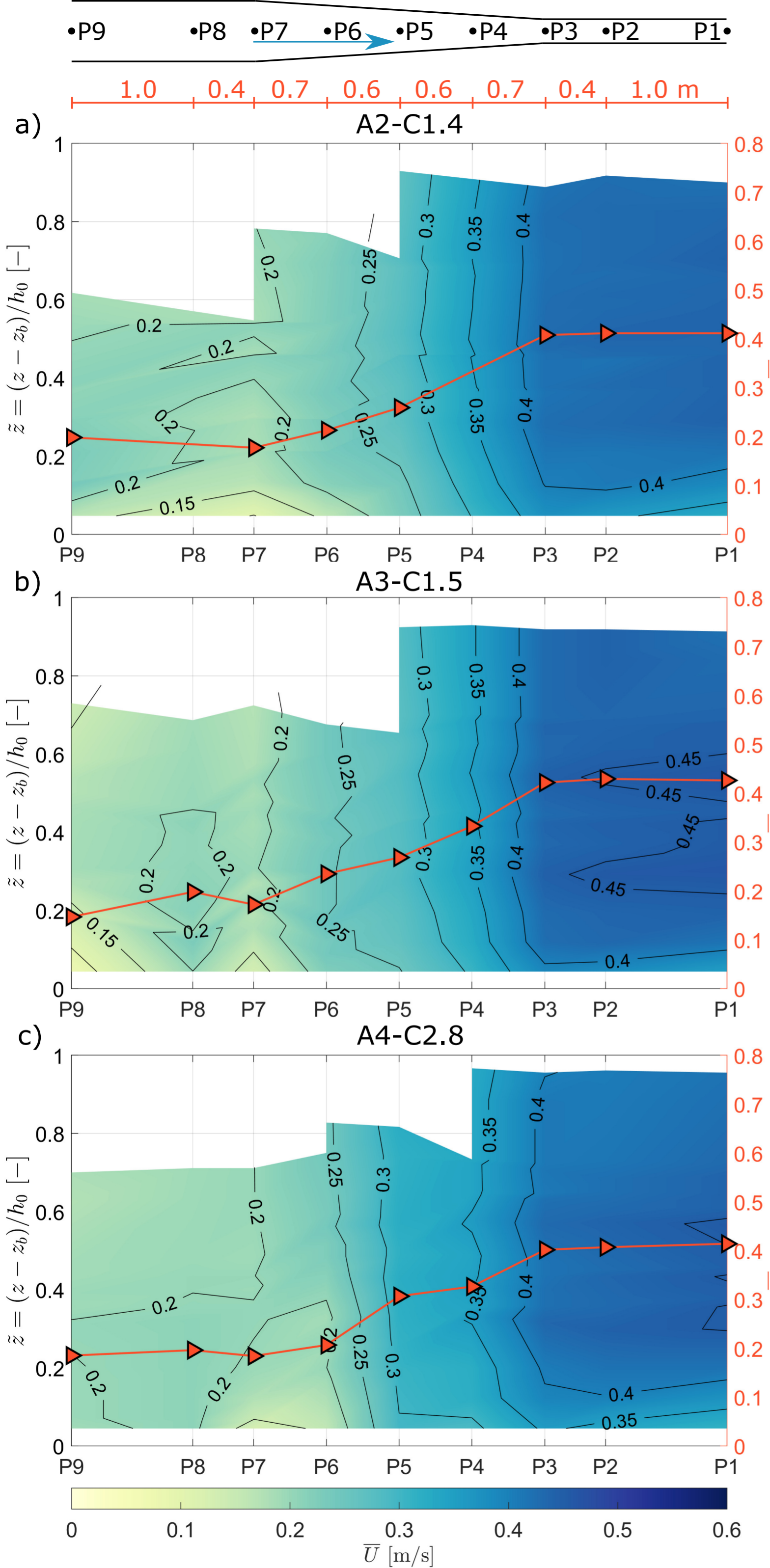
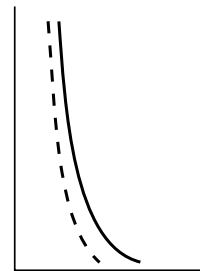


Figure8.

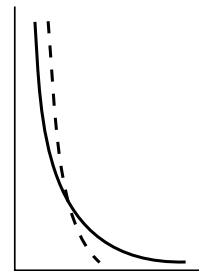
a) Turbulent flow


 $RMS(u')_0$

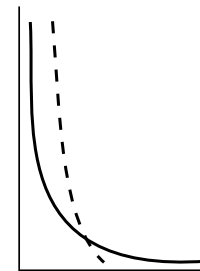
b) Turbulence-enhanced transitional flow


 $RMS(u')_0$

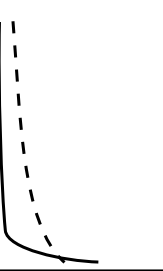
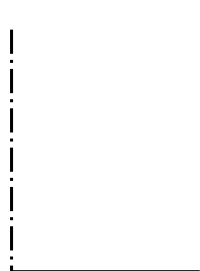
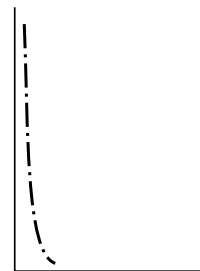
c) Lower transitional plug flow


 $RMS(u')_0$

d) Upper transitional plug flow


 $RMS(u')_0$

e) Quasi-laminar plug flow


 $RMS(u')_0$

 $\Delta RMS(u')_0$

 $\Delta RMS(u')_0$

 $\Delta RMS(u')_0$

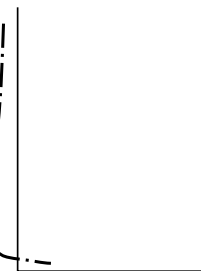
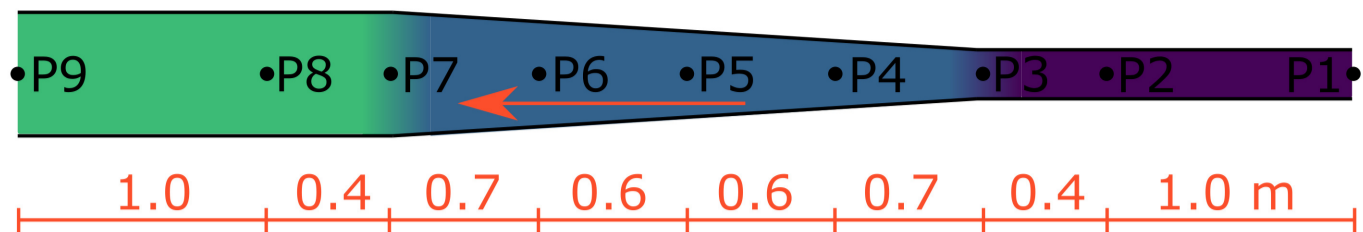
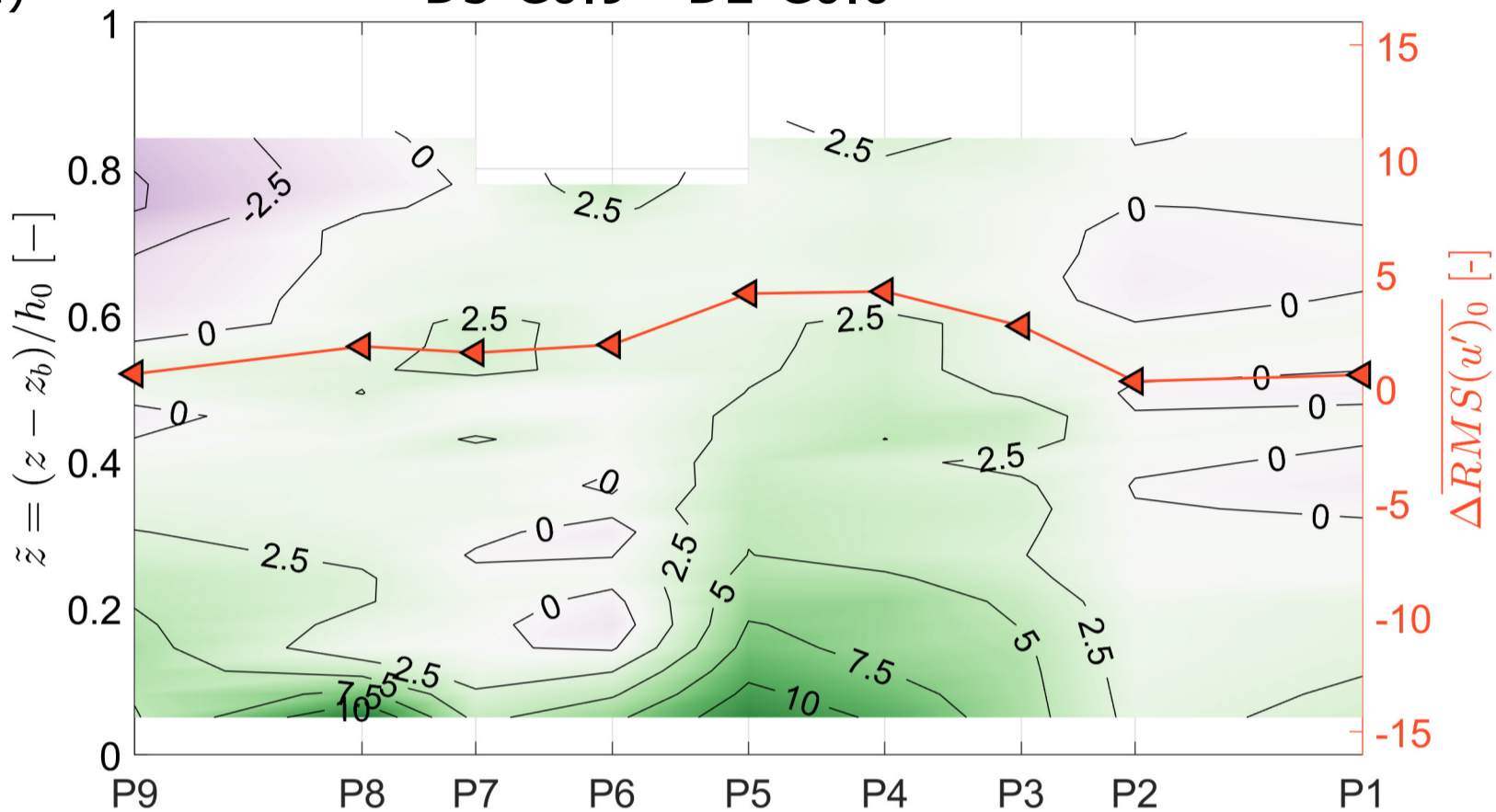
 $\Delta RMS(u')_0$

 $\Delta RMS(u')_0$

Figure9.

- Turbulent flow
- Turbulence-enhanced transitional flow
- Lower transitional plug flow
- Upper transitional plug flow



a)



b)

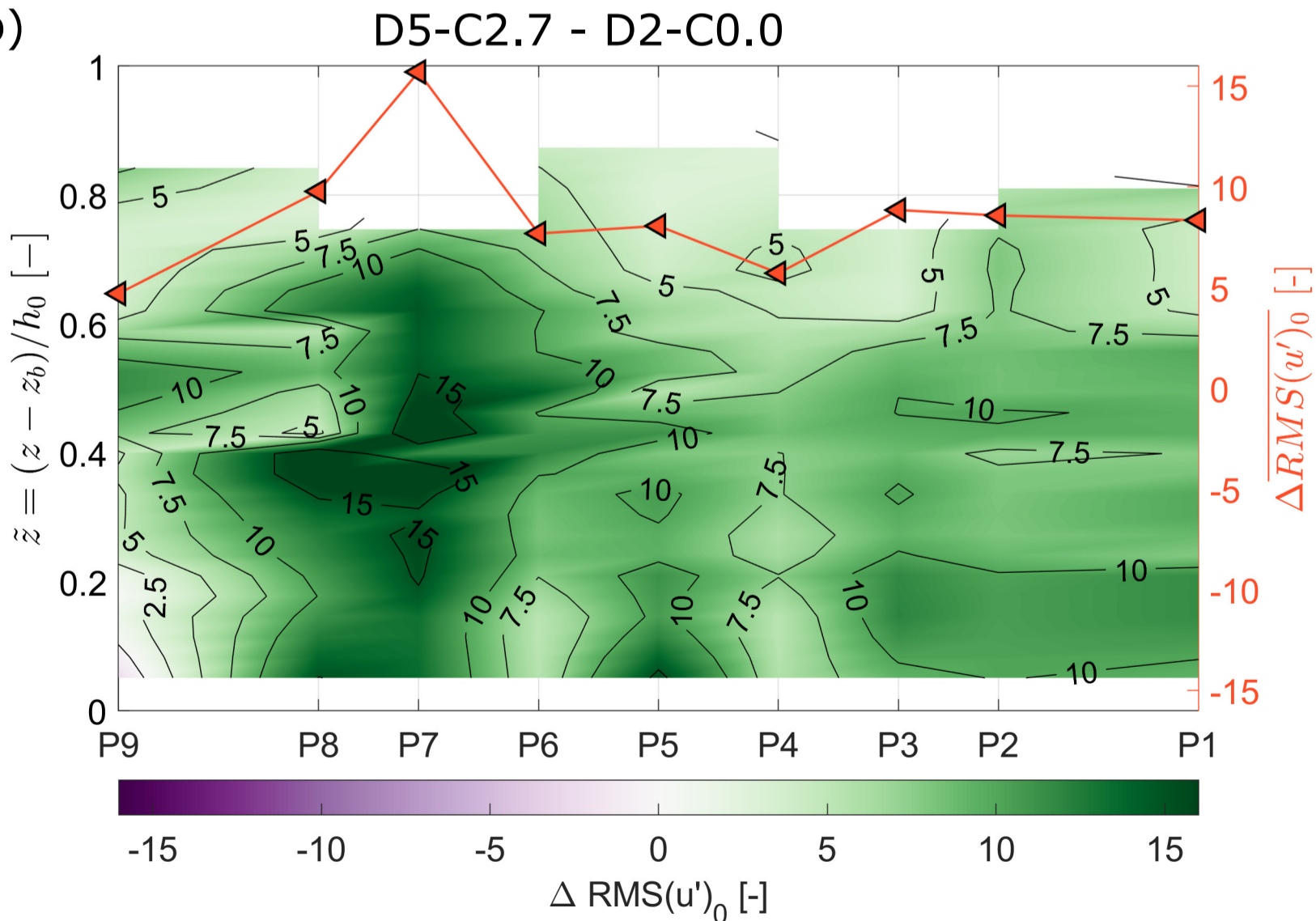
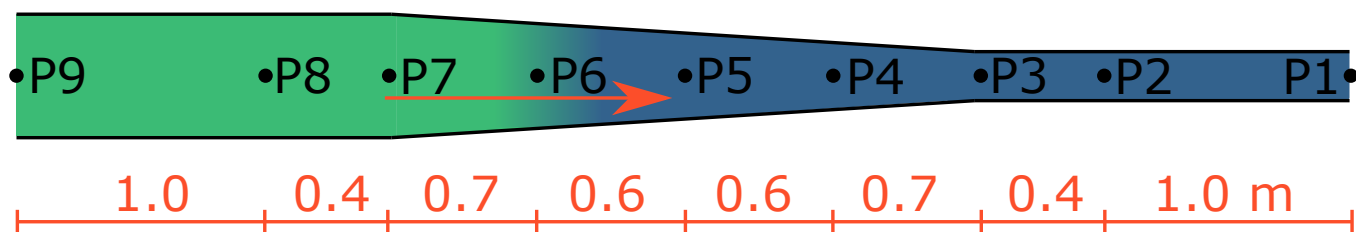
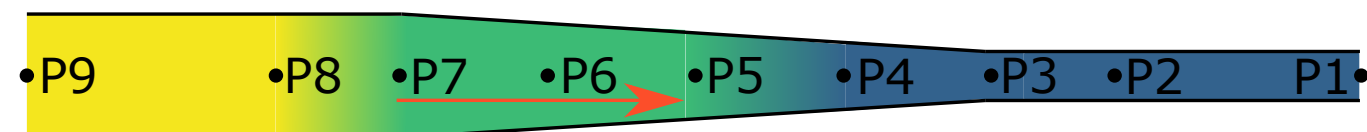
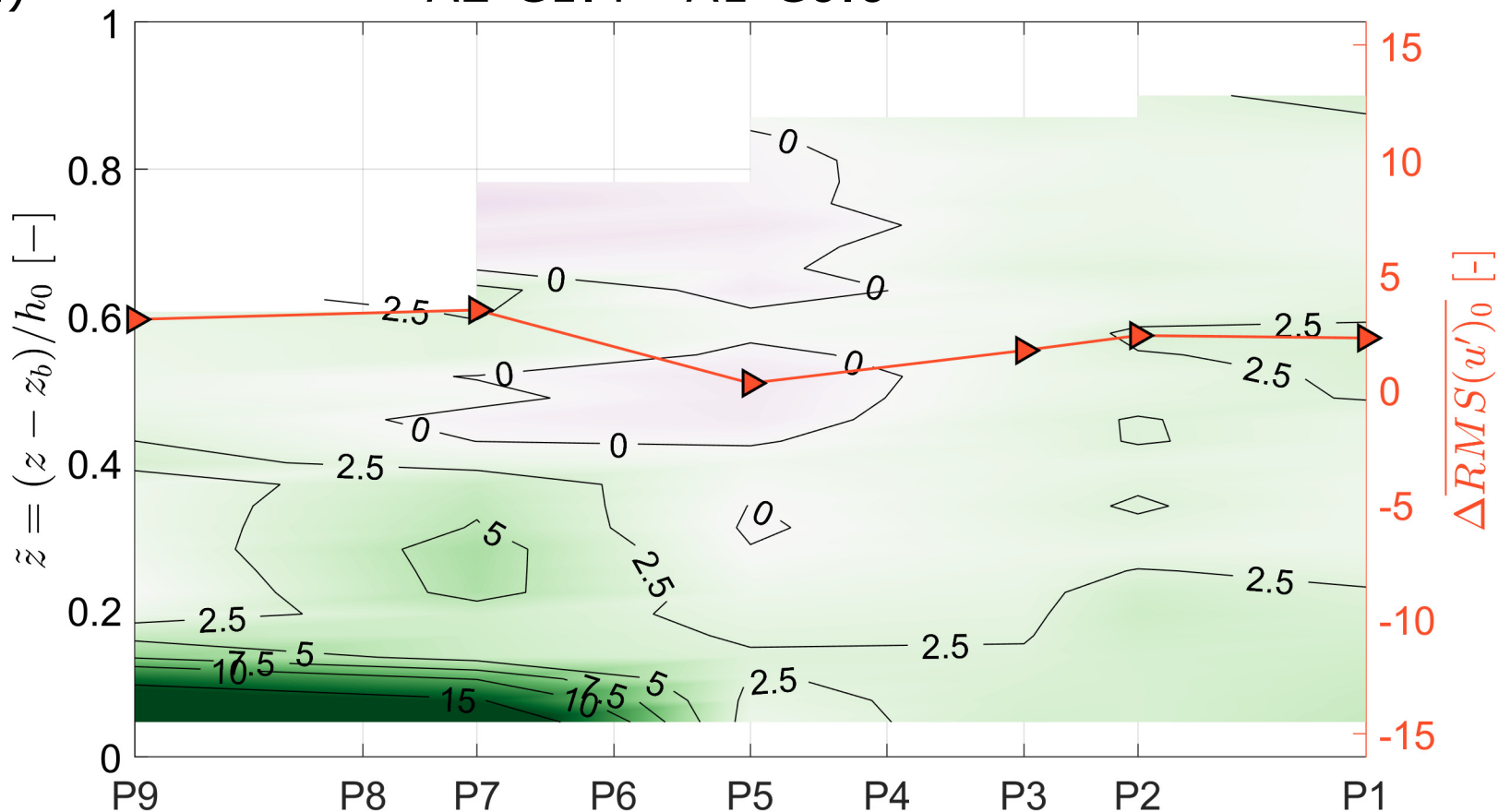


Figure10.

- Turbulent flow
- Turbulence-enhanced transitional flow
- Lower transitional plug flow
- Upper transitional plug flow



a) A2-C1.4 - A1-C0.0



b) A4-C2.8 - A1-C0.0

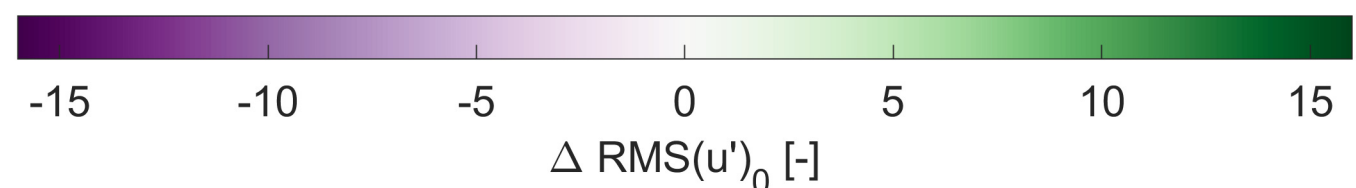
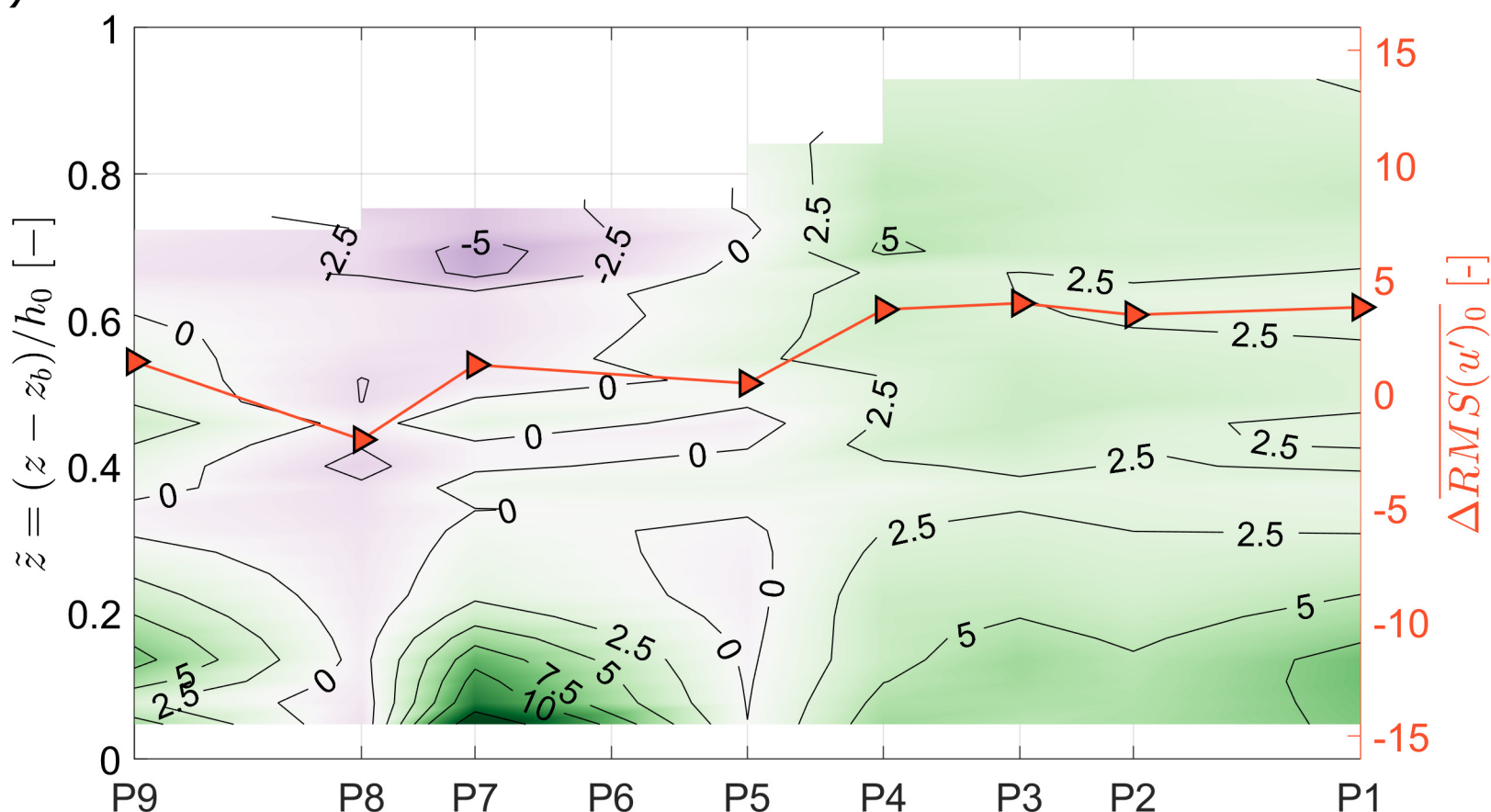


Figure11.

